ACADEMIC PRESS

Available online at www.sciencedirect.com

SCIENCE DIRECT®

Journal of Sound and Vibration 264 (2003) 49–90

JOURNAL OF SOUND AND VIBRATION

www.elsevier.com/locate/jsvi

Simplified models of the vibration of mannequins in car seats

S.K. Kim, S.W. White, A.K. Bajaj, P. Davies*

Ray W. Herrick Laboratories, School of Mechanical Engineering, Purdue University, 47907-1077 West Lafayette, IN 47907-1077, USA

Received 30 March 1999; accepted 27 May 2002

Abstract

A simplified two-dimensional modelling approach to predict the vibration response of mannequin occupied car seats about a static settling point is demonstrated to be feasible. The goal of the research is to develop tools for car seat designers. The two-dimensional model, consisting of interconnected masses, springs and dampers is non-linear due to geometric effects but, under the excitations considered, the model behaviour is linear. In this approach to modelling, the full system is initially broken down into subsystems, and experiments are conducted with subsystems to determine approximate values for the stiffness and damping parameters. This approach is necessary because of the highly non-linear behaviour of foam where stiffness changes with compression level, and because the simplified model contains more structure than is necessary to model the relatively simple measured frequency response behaviour, thus requiring a good initial starting point from which to vary parameters. A detailed study of the effects of changing model parameters on the natural frequencies, the mode shapes and resonance locations in frequency response functions is given, highlighting the influence of particular model parameters on features in the seat–mannequin system's vibration response. Reasonable qualitative as well as good quantitative agreement between experimental and simulation frequency response estimates is obtained. In particular, the two-dimensional motions at the peaks in the frequency response, a combination of up and down and rotational behaviour is predicted well by the model. Currently research is underway to develop a similar model with non-linear springs, surface friction effects and viscoelastic elements, that predicts the static settling point, a necessary step to aid in the subsystem modelling stage in this dynamic modelling approach.

1. Introduction

Car seat design is currently mostly done from experience. Both the static and dynamic response characteristics of occupied seats are important. However, in this paper only the dynamic response

*Corresponding author. Tel.: +1-765-494-9274.
E-mail address: daviesp@ecn.purdue.edu (P. Davies).

0022-460X/03/$ - see front matter
doi:10.1016/S0022-460X(02)01164-1

is focused on. Mostly, the dynamic response of seats is evaluated through tests on occupied seats where the acceleration is measured at the floor and at the seat base [1–5]. A ratio of the total weighted acceleration power at the seat base to the weighted acceleration power at the floor can be used to determine a SEAT value [1, Chapter 9, p. 405]. Car seat manufacturers would like to enhance their analytical capabilities to be able to predict seat performance prior to prototyping, and to be able to explore the effect of seat or occupant variation on the overall response. It is possible to modify the seating foam to produce different stiffness properties, but designers lack the tools to determine what stiffness variations are desirable for particular occupants. The overall objective of the research is to generate simplified two-dimensional models that predict, with reasonable accuracy, seat–occupant system dynamics and can also be used by engineers developing and troubleshooting automobile seat designs. With this objective, it is important that the elements in the model can be directly related to seat characteristics, e.g., stiffness of the foam at various locations in the seat cushion and seat back, and that it be possible to examine the effect of changes in posture and weight distribution of the occupant. The research reported in this paper is focused on modelling of seat–occupant vibration around a static settling point. Other research, not reported here, is focused on predicting the static settling point.

Many car seats consist mainly of moulded polyurethane foam blocks. Foam is a complex material that is highly non-linear, for example, the stiffness changes as a function of compression level, initially stiff then becoming soft and finally becoming stiff again as compression increases [6–10]. Different occupants will produce different levels of compression across the seat, and thus the stiffness of the seat will be different for different occupants and even for the same occupant seated in a different position. This variation can have a dramatic effect on the measured vibration responses. Foam also has a very long memory and it takes many hours for both static and dynamic steady state conditions to be achieved e.g., Refs. [7,11]. After a period of testing foam can take over 2 days to recover. If seat evaluation tests are not run until the occupant–seat system reaches steady state, then the measurements must be made at the same time in the testing procedure to achieve good repeatability. Foam properties are also sensitive to temperature and humidity [12,13], so tests should be conducted in controlled environmental conditions, and the heating of the seat from the occupant will affect the dynamic properties of the foam. All these properties of foam make it difficult to achieve repeatable results when conducting experiments.

The complexity and non-linear behaviour of the human body, see for example Ref. [1, pp. 367–369, 397], are used as arguments against the use of dummies or mannequins in place of humans in seats, and certainly the response of the human-in-seat system will differ from the mannequin-in-seat system [14,15]. Because of the complexities of foam behaviour, it is attractive to use mannequin-in-seat systems because it is much easier to control experimental parameters, and make sure that the foam deflection is consistent from test to test. Under these controlled conditions, it is possible to make consistent comparisons between two seats. This still leaves the problem of translating the differences in mannequin response into differences in human response unaddressed. Measurements of the frequency response functions of humans in seats e.g., Refs. [1,16] and mannequins in seats [17] exhibit very similar features including the number of peaks and spectral roll-off characteristics. Peak locations differ, but this is expected due to weight distribution and foam compression levels, clothing, posture, and seat type. A careful comparison of experimental results where all these features are controlled does not currently appear in the literature.

So the experimental approaches, either with humans or with mannequins, have their drawbacks. The seat designer would like to be able to do much of the seat design prior to making the seat, thus there is a need for analytical models to replace some of the experimentation. After prototyping, experimentation will still be required and thus the issues discussed above still need to be addressed. However, this paper is focused on a methodology that may be used to model a seat–occupant system undergoing base vibration. For design a model needs to be complex enough so that components in the model relate to physical properties that can be tuned in the seat manufacture, and simple enough to facilitate exploring the effects of parameter and component variation. While finite element models are being developed [18] and have been shown to work well in predicting static deflections, they currently are not sufficiently developed to predict the dynamic response accurately. When they are sufficiently sophisticated to do the dynamic predictions well, they will still be highly computationally intensive and parameter variation studies will be time-consuming and unwieldy for design. Thus, currently there is a need for simplified vibration models of seat–occupant systems.

The models described in this paper are two dimensional, planar models based on those of Nishyama [19–23] with some modifications introduced because of seat behaviour observed during experiments. The methodology is applied to a mannequin occupied seat system and it is conceivable that a similar approach may be useful for developing a simplified model of a human occupied seat system. The measured frequency responses of car-seat occupants are usually relatively simple with few peaks [16], and some researchers have used as little as two-degree-of-freedom models to fit to these frequency response functions. Others have used simple mass–spring–damper models [24–29], but it is often difficult to relate the components of these models directly to seat characteristics in a way that would be useful in seat design. A comprehensive review of the one-dimensional biodynamic human body models for this car-seat application is given by Boileau et al., in Ref. [30]. One of these one-dimensional models, the Suggs model, is used by Patten and Pang [31] who combined it with Patten's non-linear model of polyurethane foam [10] to predict vertical frequency response behaviour of a seat occupant. While illustrating the well-known non-linear behaviour of the polyurthane foam, (softening with increased amplitude of excitation) this model does not explain the two-dimensional dynamics experienced by seat occupants. As a side note, Mansfied and Griffin [32] also showed softening behaviour when measuring the response of 12 subjects seated on a seat (no seat back), but that behaviour was attributed to biodynamic effects. They also measured fore–aft response to a vertical excitation, a confirmation of the need for two-dimensional modelling approaches. The simplified two-dimensional model in this paper contains the basic components of the seat and the occupant and models the interaction (foam and soft tissue) between the two with several springs and dampers. There are geometric non-linearities in the system but the springs and dampers are assumed to be linear. This type of model is valid about an operating point and within a range of excitation levels. It has been observed that at the vibration levels typically encountered in highway driving, there is a high degree of coherence between the seat excitation and the occupant response and the relationship can be described well by a (linear) frequency response function. This is a seven-degree-of-freedom planar model and thus to produce a good fit of this model to measured data that appears much less complex, reasonable starting points for parameter values must be determined. Simply allowing the parameters to vary from random initializations may lead to unrealistic parameter values and incorrect deflection shapes. Tregoubov has pointed out a similar

problem when fitting complex one-dimensional biodynamic models to measured data [33]. A systematic way of finding good starting values through the use of tests on sub-components of the system is described and applied to the mannequin occupied seat system.

While the model is termed simplified, its behaviour is quite complex because of the strong interactions between components. The effects of many parameter variations were studied and subsets of these tests are reported in this paper. It is clear from the parameter variation studies that simplistic reasoning based on single-degree-of-freedom behaviour is not sufficient to predict the effect of changing a particular parameter in this more complicated model. This is a strong argument for the use of models in seat design to help designers understand the implications of making changes to the stiffness and damping properties of the foam.

This paper contains a description of what is required to produce a simplified model of a seat–occupant system that would be useful for a car seat designer to explore the effect of changing seat characteristics such as stiffness and damping. Whether the occupant be a mannequin or a human, a process similar to the one described is necessary if one wishes to produce good modelling tools for design prior to fabrication of prototypes.

2. The model of the seat and mannequin

The modelling approach followed here is along the lines of Nishiyama [20–22]. Based on observations of a seated mannequin's response to harmonic excitation near resonance, some modifications were made to the basic model. The geometric parameters of the model are defined in Fig. 1a, and the spring, mass, dashpot properties are defined in Fig. 1b. It was observed that at certain resonant frequencies there was significant seat back motion, whereas in Nishiyama's model the seat back was assumed to be rigidly connected to seat base. Thus, a torsional spring (k_s) was added to this connection in the present model. In some other experiments on the subsystem consisting of the seat cushion and part of the mannequin it was observed (see Section 3.4.1) that the two springs (k_3 and k_4) and dampers (c_3 and c_4), modelling the mannequin and seat cushion interaction, could not be collocated, as indicated by Nishiyama, and still correctly predict the natural frequencies and modal deformations of a loaded seat cushion. Some flexibility in the locations of these spring and damper elements was introduced so that this subsystem experiment-model mismatch could be eliminated. In the experimental configuration, the lower part of the mannequin's back did not usually touch the seat back. However, k_2 and c_2, which could be viewed as modelling the lower seat back mannequin interaction, were included in the model so that their influence could be examined. The variables k_1 and c_1 model the interaction between the upper torso of the mannequin and the upper seat back. Similarly, the variables k_5 and c_5 model the interaction of the foot with the floor. The only forcing considered here is a vertical base acceleration ($\ddot{z}$) imparted to the bottom of the seat simulating the motion of the rigid seat rails in an automobile. This is in keeping with the experimental component of the research reported here wherein the seat–mannequin system is mounted on a single axis hydraulic shaker and excited with low-frequency random noise. As in Nishiyama's work, the behaviour of the mannequin's neck, hip and knee joints was modelled by torsional dampers (T_1, T_2 and T_3) with appropriate torque–velocity relationships.

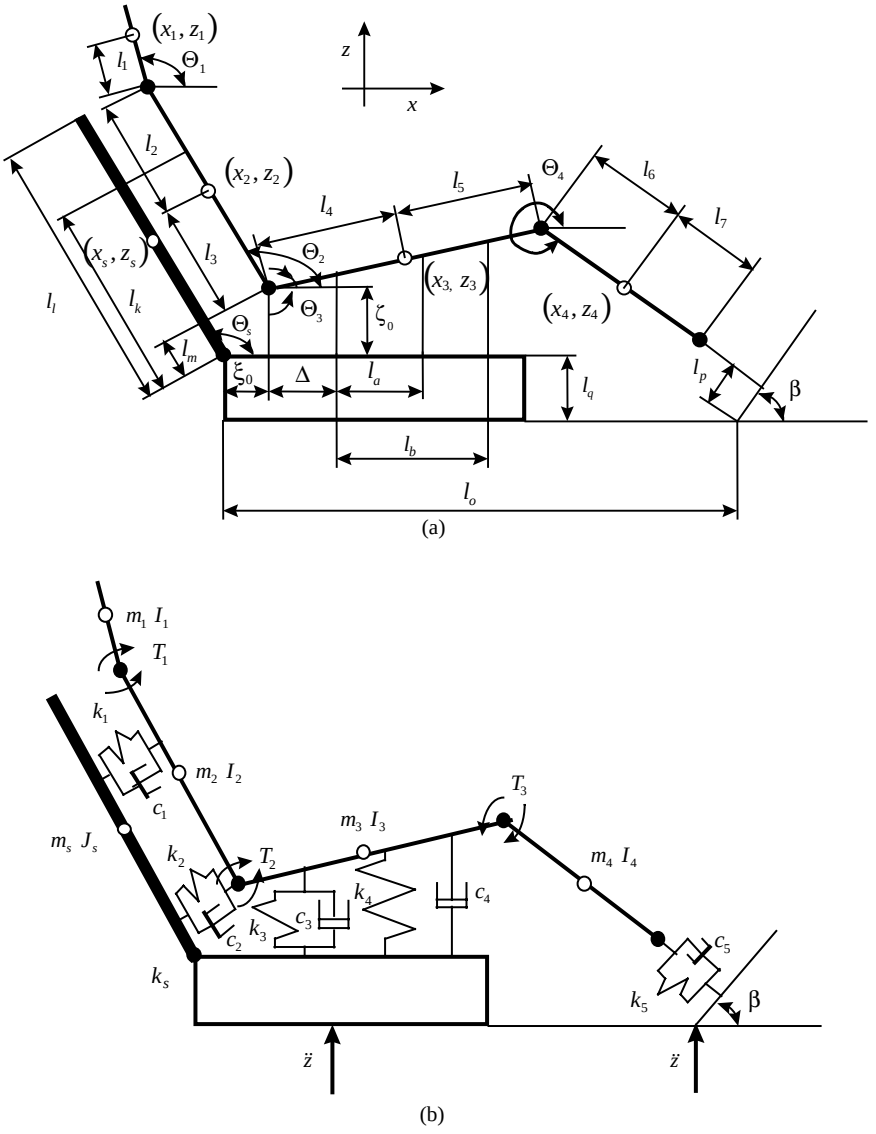

Fig. 1. Schematic of seven-degree-of-freedom model of the car seat and mannequin system. (a) Geometry and notation definition, (b) dynamic properties.

2.1. Equations of motion

All the springs and dampers, with the exception of the torsional dampers, are assumed to be linear in the modelling effort. The non-linearities in the system model come from the mannequin and seat geometry, and from the non-linear torsional dampers in the joints. The seat–mannequin system has seven-degrees-of-freedom: ξ, the absolute horizontal displacement of the hip joint; ζ, the absolute vertical displacement of the hip joint; Θ_1, the absolute angular deflection of the

neck; Θ_2, the absolute angular deflection of the torso; Θ_3, the absolute angular deflection of the femur; Θ_4, the absolute angular deflection of the knee; Θ_S, the absolute angular deflection of the seat back joint; and $\ddot{z}$, the vertical acceleration input to the seat rails. The other parameters of geometric dimensions, masses, and mass moments of inertia, are given in Table A.1 in Appendix A.

The equations of motion of the seven-degree-of-freedom model are derived by using the Lagrangian formulation. The kinetic energy, T, potential energy, U, dissipation function, D and generalized forces, Q_r, of the whole system are

$$T = \tfrac{1}{2}\sum_{i=1}^{4} m_i \dot{z}_i^2 + \tfrac{1}{2}\sum_{i=1}^{4} I_i \dot{\Theta}_i^2 + \tfrac{1}{2}\sum_{i=1}^{4} m_i \dot{x}_i^2 + \tfrac{1}{2} J_s \dot{\Theta}_s^2 + \tfrac{1}{2} m_s \dot{z}_s^2 + \tfrac{1}{2} m_s \dot{x}_s^2,$$

$$U = \tfrac{1}{2}\sum_{i=1}^{3} k_i \delta_i^2 + \tfrac{1}{2} k_4 \delta_{4k}^2 + \tfrac{1}{2} k_5 \delta_5^2 + \tfrac{1}{2} k_s \Theta_s^2, \quad D = \tfrac{1}{2}\sum_{i=1}^{3} c_i \dot{\delta}_i^2 + \tfrac{1}{2} c_4 \dot{\delta}_{4c}^2 + \tfrac{1}{2} c_5 \dot{\delta}_5^2, \tag{1}$$

$$Q_1 = 0, \quad Q_2 = 0, \quad Q_3 = -T_1, \quad Q_4 = -T_2 + T_1, \quad Q_5 = -T_3 + T_2, \quad Q_6 = +T_3, \quad Q_7 = 0,$$

where

$$x_1 = \xi + (l_2 + l_3)\cos\Theta_2 + l_1 \cos\Theta_1, \quad z_1 = z + \zeta + (l_2 + l_3)\sin\Theta_2 + l_1 \sin\Theta_1,$$
$$x_2 = \xi + l_3 \cos\Theta_2, \quad z_2 = z + \zeta + l_3 \sin\Theta_2,$$
$$x_3 = \xi + l_4 \cos\Theta_3, \quad z_3 = z + \zeta + l_4 \sin\Theta_3,$$
$$x_4 = \xi + (l_4 + l_5)\cos\Theta_3 + l_6 \cos\Theta_4, \quad z_4 = z + \zeta + (l_4 + l_5)\sin\Theta_3 + l_6 \sin\Theta_4,$$
$$x_s = 0.5 l_l \cos\Theta_s, \quad z_s = z + 0.5 l_l \sin\Theta_s.$$

(x_i, z_i), $i = 1, 2, 3, 4, 5$ define the locations of the centres of mass of the corresponding mannequin components. δ_i, $i = 1, 2, 3, 4, 5$ define the length changes in the elastic elements. Expressions for the joint torques, T_i, are given in Eq. (4). Substituting Eq. (1) into Lagrange's equations:

$$\frac{\mathrm{d}}{\mathrm{d}t}\left(\frac{\partial T}{\partial \dot{q}_r}\right) - \frac{\partial T}{\partial q_r} + \frac{\partial U}{\partial q_r} + \frac{\partial D}{\partial \dot{q}_r} = Q_r, \quad r = 1, 2, 3, \ldots, 7 \tag{2}$$

results in the following set of seven non-linear second order differential equations for the seven generalized co-ordinates ξ, ζ, Θ_1, Θ_2, Θ_3, Θ_4, and Θ_s:

$$\begin{bmatrix} -M_1 & 0 & A_1 & A_2 & A_3 & A_4 & 0 \\ 0 & -M_1 & B_1 & B_2 & B_3 & B_4 & 0 \\ D_2 & D_3 & -M_{10} & D_1 & 0 & 0 & 0 \\ E_2 & E_3 & E_1 & -M_{11} & 0 & 0 & 0 \\ G_2 & G_3 & 0 & 0 & -M_{12} & G_1 & 0 \\ H_2 & H_3 & 0 & 0 & H_1 & -M_{13} & 0 \\ 0 & 0 & 0 & 0 & 0 & 0 & -S_1 \end{bmatrix} \begin{Bmatrix} \ddot{\xi} \\ \ddot{\zeta} \\ \ddot{\Theta}_1 \\ \ddot{\Theta}_2 \\ \ddot{\Theta}_3 \\ \ddot{\Theta}_4 \\ \ddot{\Theta}_s \end{Bmatrix} = \begin{bmatrix} -A_5 \\ -B_5 \\ -D_4 \\ -E_4 \\ -G_4 \\ -H_4 \\ -S_2 \end{bmatrix}, \tag{3}$$

where

$$A_1 = M_2 \sin\Theta_1, A_2 = (M_3 + M_6)\sin\Theta_2, \quad A_3 = (M_4 + M_7)\sin\Theta_3, \quad A_4 = M_5 \sin\Theta_4,$$

$$A_5 = M_2 \cos\Theta_1\,\dot{\Theta}_1^2 + (M_3 + M_6)\cos\Theta_2\,\dot{\Theta}_2^2 + (M_4 + M_7)\cos\Theta_3\,\dot{\Theta}_3^2 + M_5 \cos\Theta_4\,\Theta_4^2 - \Delta(\xi),$$

$$B_1 = -M_2 \cos\Theta_1, \quad B_2 = -(M_3 + M_6)\cos\Theta_2,$$
$$B_3 = -(M_4 + M_7)\cos\Theta_3, \quad B_4 = -M_5 \cos\Theta_4,$$

$$B_5 = M_2 \sin\Theta_1\,\dot{\Theta}_1^2 + (M_3 + M_6)\sin\Theta_2\,\dot{\Theta}_2^2 + (M_4 + M_7)\sin\Theta_3\dot{\Theta}_3^2 + M_5 \sin\Theta_4\,\dot{\Theta}_4^2 - \Delta(\zeta) - M_1\ddot{z},$$

$$D_1 = -M_8 \cos(\Theta_1 - \Theta_2), \quad D_2 = A_1, \quad D_3 = B_1,$$

$$D_4 = -M_8 \sin(\Theta_1 - \Theta_2)\dot{\Theta}_2^2 - M_2\ddot{z}\cos\Theta_1 - \Delta(\Theta_1) - T_1,$$

$$E_1 = D_1, \quad E_2 = A_2, \quad E_3 = B_2,$$

$$E_4 = M_8 \sin(\Theta_1 - \Theta_2)\dot{\Theta}_1^2 - (M_3 + M_6)\ddot{z}\cos\Theta_2 - \Delta(\Theta_2) + T_1 - T_2,$$

$$G_1 = -M_9 \cos(\Theta_3 - \Theta_4), \quad G_2 = A_3, \quad G_3 = B_3,$$

$$G_4 = -M_9 \sin(\Theta_3 - \Theta_4)\dot{\Theta}_4^2 - (M_4 + M_7)\ddot{z}\cos\Theta_3 - \Delta(\Theta_3) + T_2 - T_3,$$

$$H_1 = -M_9 \cos(\Theta_4 - \Theta_3), \quad H_2 = M_5 \sin\Theta_4, \quad H_3 = -M_5 \cos\Theta_4,$$

$$H_4 = -M_9 \sin(\Theta_4 - \Theta_3)\dot{\Theta}_3^2 - M_5\ddot{z}\cos\Theta_4 - \Delta(\Theta_4) + T_3,$$

$$S_1 = \mathrm{J}_s + \frac{m_s l_l^2}{4}, \quad S_2 = -k_s(\Theta_s - \Theta_{s0}) - \Delta(\Theta_s) - \tfrac{1}{2} m_s l_l \ddot{z}\cos\Theta_s.$$

The Δ term in the above expressions is defined in Appendix B, and the mass parameters, M_i, are

$$M_2 = m_1 l_1, \quad M_3 = m_2 l_3, \quad M_4 = m_3 l_4, \quad M_5 = m_4 l_6, \quad M_6 = m_1(l_2 + l_3), \quad M_7 = m_4(l_4 + l_5),$$

$$M_8 = m_1 l_1(l_2 + l_3), \quad M_9 = m_4 l_6(l_4 + l_5), \quad M_{10} = I_1 + m_1 l_1^2, \quad M_{11} = I_2 + m_1(l_2 + l_3)^2 + m_2 l_3^2,$$

$$M_{12} = I_3 + m_4(l_4 + l_5)^2 + m_3 l_4^2, \quad M_{13} = I_4 + m_4 l_6^2, \quad M_1 = m_1 + m_2 + m_3 + m_4.$$

As in Nishiyama's work [20–22], the following equations were used to model the friction moments associated with each joint:

$$T_i = T_{max,i} \tanh\left(\frac{2\omega_i}{\omega_{i,0}}\right), \quad i = 1, 2, 3, \quad \text{and} \quad \omega_i = \dot{\Theta}_i - \dot{\Theta}_{i+1}, \tag{4}$$

where $T_{max,1}$, $T_{max,2}$, $T_{max,3}$ and $\omega_{i,0}$ are constants. Nishyama specified the values $T_{max,1} = 3.920\,\mathrm{N\,m}$, $T_{max,2} = 35.280\,\mathrm{N\,m}$, $T_{max,3} = 14.112\,\mathrm{N\,m}$ and $\omega_{i,0} = 0.349\,\mathrm{rad/s}$, which are most likely not appropriate for the present mannequin. The first, second and third joints of the mannequin are the neck, hip and knee, respectively, and the rotational variables in the equations (Θ_i) are defined above.

Eq. (3) was used to simulate the system response for a given vertical base acceleration, $\ddot{z}$. The simulation was programmed using MATLAB. The program was based on the fourth order Runge–Kutta integration scheme in MATLAB. Equispaced time samples were used so that frequency response functions, between the base excitation and the motions at various locations on the body, could be estimated, and compared to experimental results.

2.2. Linearized equations of motion

In general, the response of a non-linear multi-degree-of-freedom system to a random or deterministic excitation can only be evaluated by numerical simulation. Such an analysis, though realistic, does not allow the analyst to develop an in-depth understanding of the system dynamics. The non-linear simulation is also very time consuming because the results of a large number of simulations are needed to obtain a clear picture of the response dependence on model parameters. Thus, in order to reduce the analysis time for the dynamic simulations, as well as to calculate the more familiar modal properties such as the undamped natural frequencies and the mode shapes of the seat–mannequin system, linear equations of motion were derived. The geometric non-linearities were simplified by assuming small motions about the specified nominal configurations, by expanding in a Taylor series, and then retaining only linear terms in the small motion variables. In this process, the following simplifications were made:

$$\begin{aligned}&\sin\Theta_i'\approx\Theta_i', \quad \cos\Theta_i'\approx 1, \quad \sin\Theta_i=\sin(\Theta_{i0}+\Theta_i')\approx \sin\Theta_{i0}+\ \cos\Theta_{i0}\cdot\Theta_i',\\ &\cos\Theta_i=\cos(\Theta_{i0}+\Theta_i')\approx\cos\Theta_{i0}-\sin\Theta_{i0}\cdot\Theta_i',\end{aligned} \tag{5}$$

$$\sqrt{1+\ x}\approx\ 1+\ \frac{x}{2}, \tag{6}$$

$$T_i=T_{max,i}\tanh\left(\frac{2\omega_i}{\omega_{i,0}}\right)\approx 2T_{max,i}\left(\frac{\omega_i}{\omega_{i0}}\right), \quad i=1,2,3. \tag{7}$$

This linearization produces the following set of equations:

$$\begin{bmatrix} M_1 & 0 & -A_1 & -A_2 & -A_3 & -A_4 & 0\\ 0 & M_1 & -B_1 & -B_2 & -B_3 & -B_4 & 0\\ -D_2 & -D_3 & M_{10} & -D_1 & 0 & 0 & 0\\ -E_2 & -E_3 & -E_1 & M_{11} & 0 & 0 & 0\\ -G_2 & -G_3 & 0 & 0 & M_{12} & -G_1 & 0\\ -H_2 & -H_3 & 0 & 0 & -H_1 & M_{13} & 0\\ 0 & 0 & 0 & 0 & 0 & 0 & S_1 \end{bmatrix} \begin{Bmatrix} \ddot{\xi}'\\ \ddot{\varsigma}'\\ \ddot{\Theta}_1'\\ \ddot{\Theta}_2'\\ \ddot{\Theta}_3'\\ \ddot{\Theta}_4'\\ \ddot{\Theta}_s' \end{Bmatrix}$$

$$+\begin{bmatrix} K_{411} & K_{412} & K_{413} & K_{414} & K_{415} & K_{416} & K_{417} \\ K_{421} & K_{422} & K_{423} & K_{424} & K_{425} & K_{426} & K_{427} \\ K_{431} & K_{432} & K_{433} & K_{434} & K_{435} & K_{436} & K_{437} \\ K_{441} & K_{442} & K_{443} & K_{444} & K_{445} & K_{446} & K_{447} \\ K_{451} & K_{452} & K_{453} & K_{454} & K_{455} & K_{456} & K_{457} \\ K_{461} & K_{462} & K_{463} & K_{464} & K_{465} & K_{466} & K_{467} \\ K_{471} & K_{472} & K_{473} & K_{474} & K_{475} & K_{476} & K_{477} \end{bmatrix} \begin{Bmatrix} \xi' \\ \varsigma' \\ \Theta'_1 \\ \Theta'_2 \\ \Theta'_3 \\ \Theta'_4 \\ \Theta'_s \end{Bmatrix}$$

$$+\begin{bmatrix} C_{411} & C_{412} & C_{413} & C_{414} & C_{415} & C_{416} & C_{417} \\ C_{421} & C_{422} & C_{423} & C_{424} & C_{425} & C_{426} & C_{427} \\ C_{431} & C_{432} & C_{433} & C_{434} & C_{435} & C_{436} & C_{437} \\ C_{441} & C_{442} & C_{443} & C_{444} & C_{445} & C_{446} & C_{447} \\ C_{451} & C_{452} & C_{453} & C_{454} & C_{455} & C_{456} & C_{457} \\ C_{461} & C_{462} & C_{463} & C_{464} & C_{465} & C_{466} & C_{467} \\ C_{471} & C_{472} & C_{473} & C_{474} & C_{475} & C_{476} & C_{477} \end{bmatrix} \begin{Bmatrix} \dot{\xi}' \\ \dot{\zeta}' \\ \dot{\Theta}'_1 \\ \dot{\Theta}'_2 \\ \dot{\Theta}'_3 \\ \dot{\Theta}'_4 \\ \dot{\Theta}'_S \end{Bmatrix} = \ddot{z} \begin{Bmatrix} 0 \\ -M_1 \\ -M_2 \cos \Theta_{10} \\ -(M_3 + M_6) \cos \Theta_{20} \\ -(M_4 + M_7) \cos \Theta_{30} \\ -M_5 \cos \Theta_{40} \\ -0.5 m_s l_l \cos \Theta_{s0} \end{Bmatrix}, \quad (8)$$

where the terms in the coefficient matrices are defined earlier or are given in Appendix C. The 0 in the subscript denotes the nominal configuration value of the angles and a primed variable is the perturbation around the nominal value. For example, Θ_{i0} denotes the initial nominal value of Θ_i, and Θ'_i denotes the small perturbation around the nominal value.

The linear Eq. (8) depend on (1) the mass and inertia parameters for the mannequin; (2) the geometric parameters of the model; (3) the initial posture parameters; (4) the spring and damper constants modelling the car seat bottom and back-cushion; as well as, (5) the parameters defining the friction torques at the joints in the mannequin. The physical and geometrical parameters, as given in Appendix A, were available for the mannequin either from the manufacturer or by direct measurement. Parameter values in the models of the four springs and dampers that represent the car seat back and seat cushion interacting with the mannequin: k_1, k_3, k_4, k_5, c_1, c_3, c_4 and c_5 had to be estimated from experiments which are described in the next section.

2.3. Undamped natural frequencies, deflection shapes, and frequency response functions

Eq. (8) can be written as

$$\mathbf{M}\ddot{\mathbf{x}} + \mathbf{C}\dot{\mathbf{x}} + \mathbf{K}\mathbf{x} = \ddot{z}\mathbf{P} \quad (9)$$

and can be used to calculate the undamped natural frequencies (ω_i) by determining the eigenvalues (λ_i) of the matrix $\mathbf{M}^{-1}\mathbf{K}$ and noting that $\omega_i = (\lambda_i)^{0.5}$. The eigenvectors of this matrix $\mathbf{M}^{-1}\mathbf{K}$ can then be used to generate the mode shapes of the linear undamped model.

When two linear natural modes are close together and damping is significant, the deflection shape at a peak in the frequency response function is highly influenced by more than one undamped natural mode of the system. Therefore, in order to correlate the model predictions with observed motions at certain frequencies, it is useful to determine the response to a sinusoidal

excitation. This was achieved by assuming that the excitation to the seat base is harmonic: $z(t) = \exp(j\omega t)$, and finding, from Eq. (8), the amplitude and phase change of the response of each of the degrees of freedom. By using these results, the deflection of each point on the body was calculated and the operating deflection shapes were obtained.

The Laplace transform of the linearized equations including the damping terms can be used to determine the transfer functions between the base excitation and the responses. Taking the Laplace transform of Eq. (9), and assuming zero initial conditions, yields

$$\mathbf{X}(s) = [\mathbf{M}s^2 + \mathbf{C}s + \mathbf{K}]^{-1}[s^2 Z(s)\mathbf{P}], \tag{10}$$

where $\mathbf{X}(s)^{\mathrm{T}}$ is $\{\zeta(s), \xi(s), \Theta_1(s), \Theta_2(s), \Theta_3(s), \Theta_4(s), \Theta_s(s)\}$. The frequency response function relating the base acceleration to the second derivative of the state parameters $\{\zeta, \xi, \Theta_1, \Theta_2, \Theta_3, \Theta_4, \Theta_s\}$ can be found by substituting $s = j\omega$ into the above equation, which yields the frequency response function vector,

$$H(j\omega) = [-\omega^2\mathbf{M} + j\omega\mathbf{C} + \mathbf{K}]^{-1}\{-\omega^2\mathbf{P}\}. \tag{11}$$

In experiments, $\ddot{\varsigma} + \ddot{z}$, the absolute vertical acceleration at the hip joint, is measured. The frequency response function relating base acceleration ($\ddot{z}$) to absolute vertical acceleration is simply calculated by adding 1 to the corresponding relative motion frequency response function.

3. Mannequin and seat properties and initial model parameters

3.1. Experimental set-up and measurements

Car-seat foam behaviour is complex and realistic models of the foam relaxation behaviour [6–8] should include terms with very long time constants. This behaviour requires that care be taken in establishing repeatable measurement procedures involving time for the system to come to both static and dynamic steady state before measurements are taken [11,17]. Posture also affects the response of the seat–mannequin system [19] and hence effort was made to ensure that the mannequin was positioned in the same position and orientation in the seat. The experimental configuration for the vibration testing is shown in Fig. 2. Low-frequency Kistler, Type 8303, and Neuwghent SAA-1000 accelerometers were used to measure the acceleration on the seat rails and on various parts of the mannequin. While the foam is truly non-linear [9,11], at the low levels of base acceleration typically measured on car seat rails during highway driving, the relationship between the seat rail acceleration and the seat–occupant vibration can be modelled with linear models for a particular seat–mannequin configuration. In Fig. 3 are shown frequency response functions between the acceleration at the seat rails and the vertical accelerations at the mannequin's bottom, back, and knee, as estimated from a test with the seat–mannequin system on the hydraulic shaker. The excitation at the seat rail was a low-frequency random input in the frequency range 3–35 Hz. The low level of excitation below 3 Hz resulted in an input signal to noise ratio that progressively decreased as the frequencies approached 0 Hz; this has the effect of biasing the frequency response function (input to output cross-spectral density/input power spectral density) away from the true value, which should be close to 1 at low frequencies. Therefore, information in the frequency response plots below 3 Hz should be ignored. The

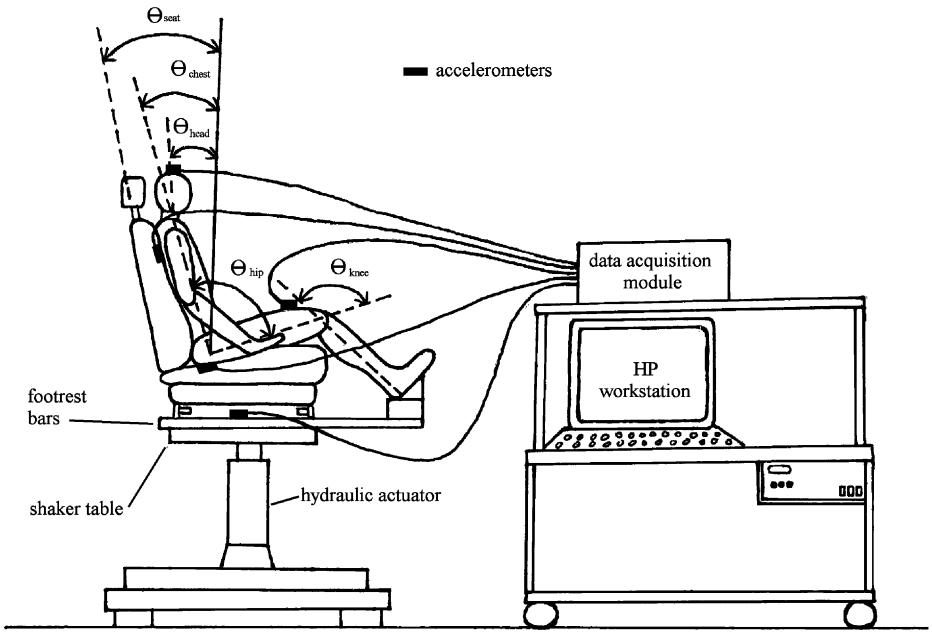

Fig. 2. Experimental set-up of the car–seat and mannequin system. The standard mannequin position corresponds to: $\theta_{head} = 10^\circ$, $\theta_{chest} = 20^\circ$, $\theta_{seat} = 20^\circ$, $\theta_{hip} = 96^\circ$, and $\theta_{knee} = 126^\circ$, and ξ_0, the horizontal distance from the seat back to the mannequin bottom location = 0.165 m.

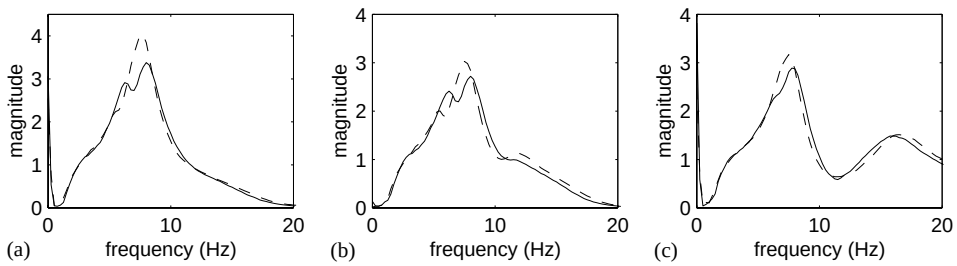

Fig. 3. Estimated frequency response magnitudes for the seated mannequin with and without head attached. (a) Rail to bottom, (b) rail to back, and (c) rail to knee frequency response functions. Solid line: with head; dashed line: without head.

frequency response functions were estimated by using a segment averaging approach, using 2048 data point segments, a Hann window, and 50% overlapping segments [34]. The sample rate was 512 samples per second and thus the frequency resolution was 0.25 Hz.

The neck joint of the mannequin used was problematic. During dynamic testing it tended to become loose and the mean angular orientation moved away from its initial orientation; it is not a realistic representation of a person's neck joint. To remove this uncontrollable variability in the experiment, dynamic tests were performed with the head and neck removed. Modelling was then

focused on the response of the seat and headless mannequin system. In Fig. 3 are shown the measured frequency response functions, both with and without the mannequin's head attached.

When the mannequin's head is removed, the peak response at the bottom, knee, and back are all seen to increase in magnitude. There is also a slight shift downward in the frequency of the largest peak response, from about 8 Hz to near 7.5 Hz. The secondary peak also decreases in its frequency, from about 6.5 to 5.5 Hz, but unlike the largest peak, its amplitude is seen to decrease. With the head removed, the downward shift in frequency might seem counterintuitive. The removal of mass is commonly associated with an increase in frequency, since for a single-degree-of-freedom system, the natural frequency would indeed increase with less mass. However, the head and neck are not simply a mass element, and the system that they are part of is very complicated. The head and neck possess certain rotational stiffness and damping properties, and their effect on the system is difficult to predict.

3.2. Modification of the mannequin model

In order to account for the head removal, the head mass, m_1, mass-moment-of-inertia, I_1, and the frictional damping force in the neck joint, T_1, were set to zero in the model. This resulted in a six-degree-of-freedom model which is obtained from Eq. (8) by eliminating the variable Θ_1. For this equation also, the linear equations of motion were derived in order to determine the undamped natural frequencies, mode shapes and frequency response functions. The same assumptions regarding small motions, as described earlier, were used to obtain the linear equations of motion.

3.3. Mannequin deflection shapes

In order to more accurately assess the actual deformations at frequencies where peaks occur in the frequency response function magnitude, and to compare with the response of the analytical linear as well as non-linear models, a stroboscope was used to visualize the mannequin motion. The seated mannequin was excited with a single frequency very close to a resonance, and the strobe light was triggered at a slightly higher frequency. These tests were performed with and without the mannequin's head attached. A graphical representation of the observed deflections at the two resonances are shown in Fig. 4 (mannequin with head) and Fig. 5 (mannequin without head).

With the head attached, the higher frequency (bounce) mode at 8 Hz is indeed seen to contain mostly vertical motion, with the mannequin mainly sliding up and down along the incline of the seat back. The shoulders remain in contact with the seat back, but the hip joint moves in a strictly vertical direction, rather than just sliding in unison with the shoulders. For this reason, a small angular motion of the torso is also induced. Similarly, the head moves mostly along the plane of the seat incline, with only a small amount of angular motion. However, the head's angular motion is out of phase with the torso's angular motion. The motion of the knees consists of small displacement due to the movement of the hips, and the mannequin's hands simply bounce on the seat cushion in unison with the hips. The material at the soles of the feet is also seen to compress slightly against the foot rests as the mannequin bounces.

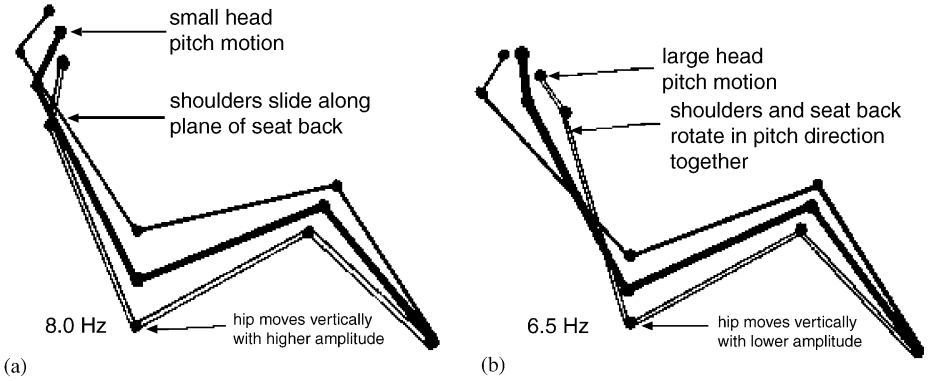

Fig. 4. Deflection shapes at (a) 8.0 Hz "bounce mode", and (b) 6.5 Hz "pitch mode" for the mannequin with head attached.

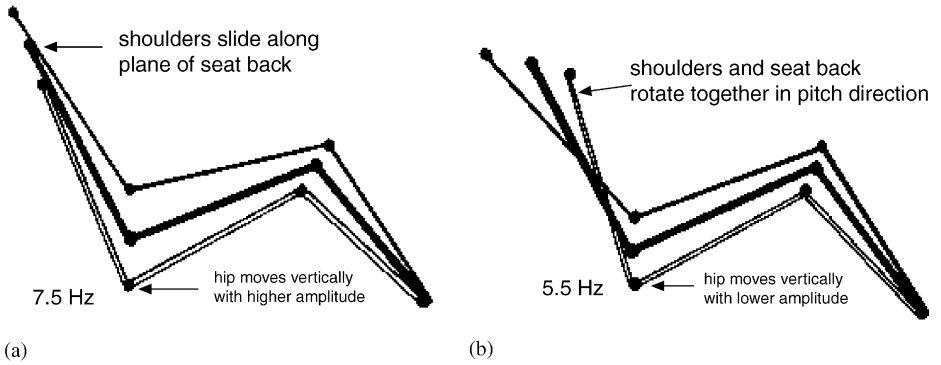

Fig. 5. Deflection shapes at (a) 7.5 Hz "bounce mode", and (b) 5.5 Hz "pitch mode" for the mannequin without head attached.

The pitch mode at 6.5 Hz is characterized by larger angular motion of the mannequin and seat back in the pitch direction. In this mode, the torso still slides along the seat back and the hips still move vertically. However, the torso and seat back also move together in the pitch direction. Accordingly, the head exhibits much larger motion than in the bounce mode, and is again out of phase with the torso. As before, the knees and arms show little additional motion of their own.

When the head is removed, the amplitudes of the motions and the resonance frequencies change. However, the character of the motion of the remaining parts of the mannequin at resonance changes very little: the two primary mannequin deflection shapes, as shown in Fig. 5, indicate motions that involve the seat back and mannequin rotating together; this is primary motion at the lower frequency (5.5 Hz). This is one of the primary observations that prompted the addition of a torsional spring, k_s, to the model at the junction of the seat back and seat cushion. It was believed that with this modification to the Nishiyama model, seat back motions could also be predicted by the simplified system model.

3.4. Experimental estimation of model parameters

The simplified model being used is shown in Fig. 1(b). The parameters k_1, c_1, k_3, c_3, k_4, c_4, k_5, k_s and J_s have to be experimentally determined. The parameters k_2 and c_2 were initially estimated to be zero, since during the experiments, it was observed that the mannequin did not make contact with the seat back in the lower back area.

3.4.1. Measurement of k_3, c_3, k_4 and c_4

The hips and thighs of the mannequin were separated from the rest of the mannequin and placed in the seat. The hips and thighs were weighted to reproduce the deflection pattern in the seat cushion, as if the entire mannequin were seated. A static finite element analysis of the seat–mannequin system (developed at Johnson Controls, Inc. [18]) was used to determine this mass distribution on the mannequin's hips and thighs. Two masses were added to the system, as shown in Fig. 6. The size and locations of these blocks were varied until the finite element predicted deflections matched those produced when the full mannequin was in the seat. Earlier, the static response predictions from the finite element formulation had been shown to agree well with static deflections and pressure distributions measured in experiments.

After the system had reached a static steady state (this takes approximately 30 min because of long-term memory effects, or creep, in the foam), it was exercised for 10 min by exciting the system with a random base excitation. The partial mannequin system was then given initial conditions such that it responded in one of its natural modes of vibration. For motion of the system in the vertical/fore–aft plane, there are two primary natural modes for this system. The lowest frequency mode consisted of mostly angular motion of the mannequin section (the pitch mode), and the higher frequency mode consisted of primarily vertical motion (the bounce mode).

The acceleration response time histories were measured at the butt and at the knee, for the two sets of initial conditions. From these measurements, the vertical and rotational accelerations could be calculated. These time histories were used to evaluated the parameters k_3, k_4, c_3 and c_4 such that, with given values of the mass, M_T, and the moment of inertia, J_T, the two-degree-of-freedom model in Fig. 6(a) responds with the same two natural frequencies, mode shapes, and vibration

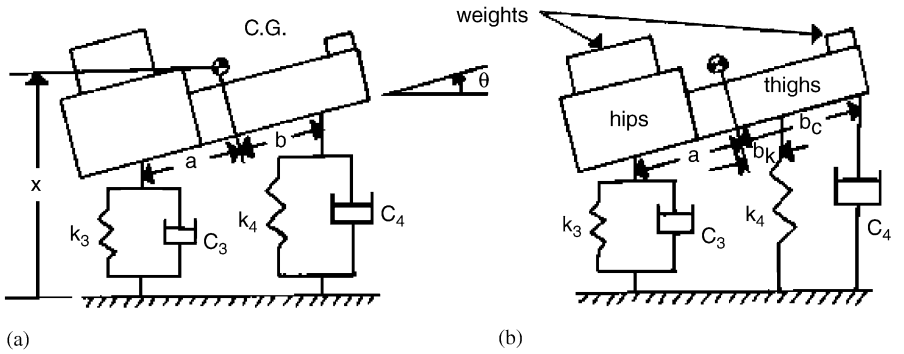

Fig. 6. (a) First simplified model of mass-loaded partial mannequin seat cushion system with collocated springs and dampers, and (b) mass–spring–damper model of the system with flexible spring and damper locations.

decay rates as the experimental system. However, it was found that in the configuration shown in Fig. 6(a), it was not possible to solve for all the parameters and constrain the system to have the correct modal deflections. The model shown in Fig. 6(b) was then adopted whereby the spring and damper number 3 remained collocated, while the spring and damper number 4 were in different positions. Using this configuration, a model could be estimated that reproduced the motions measured in the experiment.

The equations of motion, in matrix form, of the two-degrees-of-freedom shown in Fig. 6(b) are

$$\begin{bmatrix} M_T & 0 \\ 0 & J_T \end{bmatrix} \begin{Bmatrix} \ddot{x} \\ \ddot{\theta} \end{Bmatrix} + \begin{bmatrix} c_3 + c_4 & b_c c_4 - a c_3 \\ b_c c_4 - a c_3 & b_c^2 c_4 + a^2 c_3 \end{bmatrix} \begin{Bmatrix} \dot{x} \\ \dot{\theta} \end{Bmatrix} + \begin{bmatrix} k_3 + k_4 & b_k k_4 - a k_3 \\ b_k k_4 - a k_3 & b_k^2 k_4 + a^2 k_3 \end{bmatrix} \begin{Bmatrix} x \\ \theta \end{Bmatrix} = \begin{Bmatrix} 0 \\ 0 \end{Bmatrix}. \tag{12}$$

These equations of motion contain off-diagonal coupling terms in both the damping and stiffness matrices. When the mass-loaded seat cushion system (Fig. 6) was displaced vertically the response was predominantly in the vertical direction, and only a small amount of rotation was observed. The system could also be excited so that a pitch-only response was observed, however, the rotation in this case was not exactly around the centre of mass. This clearly indicates the coupling between the bounce and pitch modes. However, since the intent of this analysis was to obtain approximate values for k_3, k_4, c_3, and c_4, it is reasonable to make the assumption that the two modes are uncoupled. Thus,

$$b_c c_4 - a c_3 = 0, \quad b_k k_4 - a k_3 = 0. \tag{13}$$

The equations of motion (12) then become uncoupled and the first and the second equations describe the bounce and the pitch modes, respectively. The frequencies (ω_b and ω_p) and damping ratios (ζ_b and ζ_p) for both the bounce and pitch modes were estimated from measured data by using Prony series modelling [35]. Equating these estimates to the natural frequencies and damping ratios predicted from Eq. (12) gives

$$\begin{aligned} &c_3 + c_4 = 2M_T \varsigma_b \omega_b, \quad k_3 + k_4 = M_T \omega_b^2, \\ &b_c^2 c_4 + a^2 c_3 = 2J_T \varsigma_p \omega_p, \quad b_k^2 k_4 + a^2 k_3 = J_T \omega_p^2. \end{aligned} \tag{14}$$

There are 6 equations and 7 unknowns: a, b_c, b_k, k_3, k_4, c_3, and c_4. The original model had one set of springs and dampers located at the mannequin's bottom. It was decided to keep this spring and damper (c_3 and k_3) in the same location, and allow the location of c_4 and k_4 to vary. Thus, the parameter a was fixed and the rest were solved for. The results were $a = 0.139\,\text{m}$ (defined), $b_c = 0.134\,\text{m}$, $b_k = 0.035\,\text{m}$, $l_a = a + b_k = 0.174\,\text{m}$, $l_b = a + b_c = 0.273\,\text{m}$ (Fig. 1), $c_3 = 151.4\,\text{N s/m}$, $c_4 = 157.2\,\text{N s/m}$, $k_3 = 16,239\,\text{N/m}$, and $k_4 = 64,548\,\text{N/m}$. The free vibration response for both natural modes of vibration of the partial mannequin and of the estimated model are shown in Figs. 7(a) and (b).

At first glance a k_4 value around four times a k_3 value seems surprising. However, this is not unreasonable if one considers the non-linear behaviour of polyurethane foam [9]. Polyurethane foam's stiffness changes with compression. At small compression (0–15%, the bending region) the foam has high static stiffness. At larger compressions (15–55%, the buckling region) the foam becomes much softer, but above this the foam becomes highly compacted (the densification

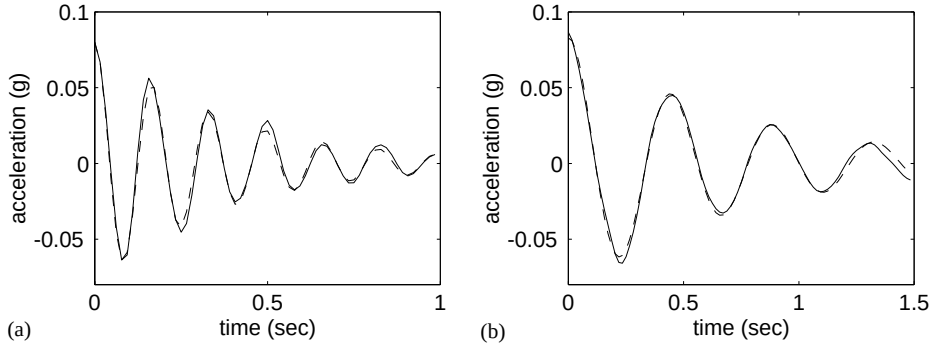

Fig. 7. (a) Bounce mode response at the knee, and (b) pitch mode response at the knee. Solid line: measurement; dashed line: model.

region) and the stiffness again increases. With the mannequin, the compression under the tuberosities (close to the location of k_3 in the model) is in the mid-range, while under the thighs (close to the location of k_4 in the model) the compression is much smaller and in the first region. Thus, k_3 nearly four times k_4 is consistent with foam behaviour.

3.4.2. Measurement of k_5

Now consider the stiffness and the damping at the interface between the mannequin's foot and the rigid supports, k_5 and c_5. The mannequin's shin consists of a metal bar surrounded by foam rubber. However, since the bar does not extend past the heel, the majority of the flexing in the shin element occurs at the mannequin's foot, which is made entirely of the foam rubber. Thus, compression of the entire shin element is approximately equivalent to compression of the mannequin's foot because the rest of the shin is nearly rigid in comparison.

The mannequin's shin was removed and placed axially in a hydraulic press. A schematic of the test set-up is shown in Fig. 8(a). Several tests were conducted where the force–displacement relations for the mannequin's foot (in the axial direction) were evaluated. In the mannequin–seat system the foot was resting on a footrest without any additional clamping. The foot remained in contact with the footrest during the vibration experiments. The compression in the leg during the experiments was small and in the range used in the static deflection test. The averaged value of the stiffness, for compressions between 1.27 mm (0.05″) and 2.54 mm (0.25″), was used to represent the net stiffness of the mannequin's foot. The results of the tests are shown in Fig. 8(b). Clearly, this measurement of the static stiffness will not yield the exact dynamic stiffness, since the foot is itself made from a foam-type material and hence exhibits viscoelastic behaviour. However, the results should be sufficient as a starting point for the modelling of mannequin used in this research. The estimated stiffness at the foot was $k_5 = 15,279\,\mathrm{N/m}$. The damping value for c_5 was specified as in Nishiyama's work due to the lack of any other rational basis to determine its value.

3.4.3. Measurement of k_1 and c_1

The mannequin was loaded into the seat in the standard position, see Fig. 2. Sheets of paper were taped to the mannequin's upper back, and to the surface of the seat back. By spray painting

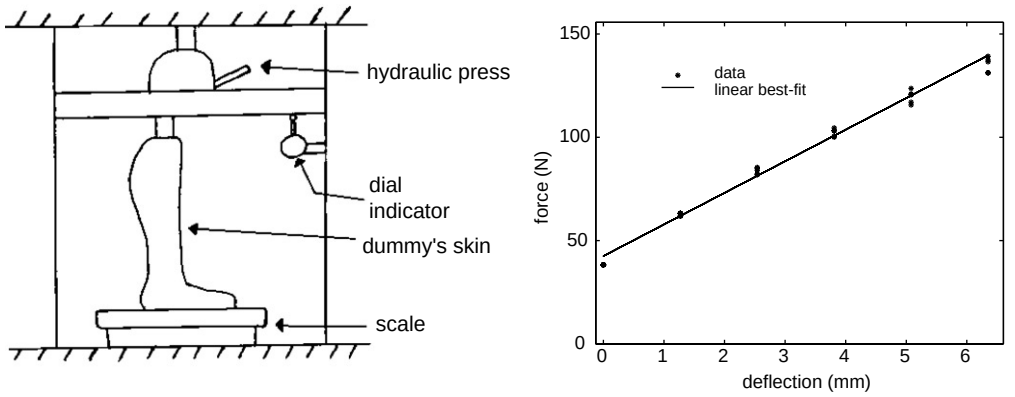

Fig. 8. (a) Schematic of test to identify stiffness of the mannequin's foot, and (b) measured compression plotted versus force, and straight line approximation.

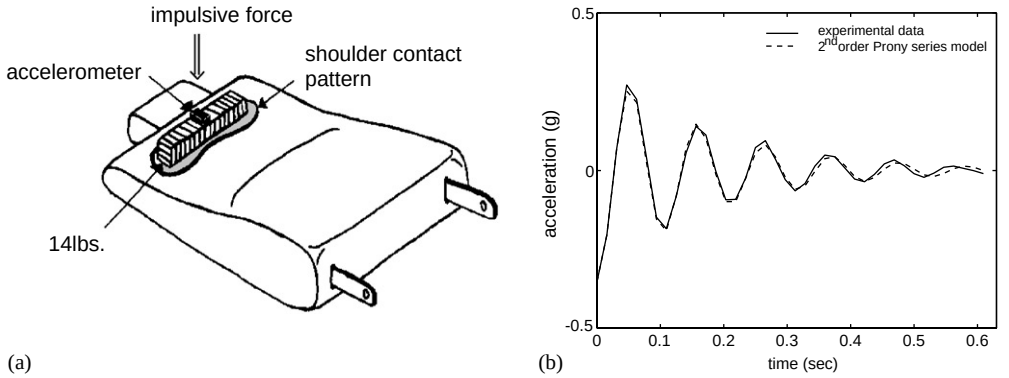

Fig. 9. (a) Schematic of experimental set-up for determination of k_1 and c_1. (b) Measured and modelled free vibration response of mass loaded seat back system.

the paper on the mannequin's upper back and then allowing it to sink in and rest on the seat back, an estimate of the contact area between the mannequin's back and the seat back was obtained. Then, in order to estimate the approximate force exerted by the seated mannequin on the seat back, a linear force gage was attached to the mannequin's shoulders and used to pull the torso until it just lost contact with the seat back. The force sustained by the foam underneath the upper back contact area was estimated to be 6.356 g N. In Fig. 9 is shown the experimental set-up that was used to determine the free response needed to estimate the parameters k_1 and c_1.

A 6.4 kg metal mass was fabricated, such that its profile matched the contact area of the mannequin on the seat back. This mass was made such that it was symmetrical along all axes. The seat back was removed from the base and placed flat on a table. The mass, with an accelerometer attached, was placed in the appropriate location on the seat back and allowed to settle for 20 min. The mass was given an impulse excitation and the resulting response was recorded. The impulse

excitations were imparted so as to generate only translational, vertical motion and minimize the angular motion of the mass. The free vibration time histories were then modelled as a single damped sine wave, and using the mass, the net stiffness and damping values were estimated to be $k_1 = 23,059\,\mathrm{N/m}$ and $c_1 = 70.48\,\mathrm{N\,s/m}$, respectively. The foam was not exercised prior to transient testing, because that would have required fabrication of a special fixture to attach the seat back to the shaker and this may change the response characteristics of the seat back.

3.4.4. Measurement of k_s

The seat back was removed and weighed. Then, the moment of inertia of the seat back about its attachment point and the location of its centre of gravity were determined. To determine these parameters, the seat back was simply hung and allowed to swing freely under gravity as shown in Fig. 10(a).

For small angular displacements, a linear equation of motion can easily be derived for the system shown in Fig. 10(a) when hung from each of the two suspension points; the corresponding natural frequencies of oscillation are given by

$$\omega_1^2 = \frac{m_s g L_G}{J_G + m_s L_G^2}, \quad \omega_2^2 = \frac{m_s g (l_l - L_G)}{J_G + m_s (l_l - L_G)^2}, \tag{15}$$

where m_s is the total mass of the seat back (4.77 kg), g is the acceleration due to gravity ($9.81\,\mathrm{m/s^2}$), L_G is the distance from the attachment point O to the centre of gravity, L is the total height of the seat back (0.8 m), and J_G is the moment of inertia about the centre of gravity. By using the two measured natural frequencies and Eq. (15), J_G and L_G were found to be: $L_G = 0.40\,\mathrm{m}$, and $J_G = 0.24\,\mathrm{kg\,m^2}$. Finally, the moment of inertia about the attachment point, J_s, was then calculated to be $1.0\,\mathrm{kg\,m^2}$.

In order to determine the stiffness of the torsional spring needed to model the attachment point, the model shown in Fig. 10(b) was used. From the linearized equation of motion about Θ_0, the

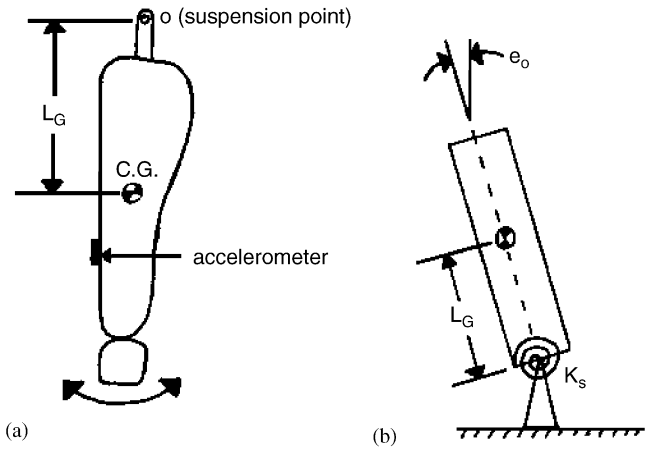

Fig. 10. (a) Experimental configuration used to measure seat back inertial properties. (b) Simplified model used in estimating the seat back torsional stiffness.

natural frequency of the seat back rotation is given by

$$\omega_n^2 = k_s/J_s. \tag{16}$$

From tests on the unoccupied seat, the natural frequency of the seat back in the pitch direction was known to be about 13.5 Hz. Using this information along with the moment of inertia J_s, it was possible to solve for the unknown torsional stiffness k_s, which was estimated to be 7194.94 N/rad.

3.5. Model parameters based on subsystem parameter estimates

The results of the experiments described above are summarized in the Table 1. In the rest of paper, this is referred to as the baseline model. In the following section of the paper, the effects on the frequency response functions of variations around these experimentally determined values for stiffness and damping will be explored, in addition to investigating the effect of variations in the damping in the mannequin's joints.

4. Simulation results

In the following sections, the effects on the seat–mannequin system's undamped natural frequencies, linear mode shapes, and the frequency response functions, due to changes in the stiffness and damping parameters will be examined. Each of these characteristics are affected in a different way by the changes in the parameters. Therefore to get a full picture of the implication of changing a parameter, it is important to investigate the changes in all of these characteristics. The studies described in this section are based on baseline parameter values determined by the subsystem evaluations, and linear model predictions are used to assess the effects of the parameter variations.

4.1. The effect of changing the positions of k_3, c_3, k_4 and c_4

The following equations are based on the modelling of the seat cushion subsystem, as described in Section 3.4.1. From these equations, and with reference to Fig. 1, k_3, c_3, k_4 and c_4 can be

Table 1
Spring stiffness and damping coefficient values determined experimentally. c_5 was chosen to be 80 c_1 based on the ratios used by Nishiyama. These are the baseline model parameters

Spring stiffness (N/m)		Damping coefficient (N s/m)	
k_1	23,059	c_1	70.48
k_2	0.00	c_2	0.00
k_3	16,239	c_3	151.38
k_4	64,648	c_4	157.16
k_5	15,279	c_5	5638.40
k_s	7194		

calculated if the distances between the positions of k_4 and c_4, b_k and b_c, respectively, and the position of centre of gravity of the seat bottom are defined (Fig. 6(b)). In the calculations, k_3 and c_3 are located in the same position and $a = a_{k3} = a_{c3} = (0.139 - \Delta)$ m. The default location for k_3 and c_3, their position in Nishiyama's model, corresponds to $\Delta = 0$ m. Once a is specified the other parameters can be solved for, as follows:

$$k_3 = \frac{J_T M_T \omega_b^2 \omega_p^2}{(a^2 M_T \omega_b^2 + J_T \omega_p^2)}, \quad k_4 = \frac{a^2 M_T \omega_b^2}{(a^2 M_T \omega_b^2 + J_T \omega_p^2)}, \tag{17}$$

$$c_3 = \frac{2 J_T M_T \omega_b \omega_p \varsigma_b \varsigma_p}{a^2 M_T \omega_b \varsigma_b + J_T \omega_p \varsigma_p}, \quad c_4 = \frac{2 a^2 J_T M_T \omega_b^2 \varsigma_b^2}{a^2 M_T \omega_b \varsigma_b + J_T \omega_p \varsigma_p}, \tag{18}$$

$$l_a = a + \frac{J_T \omega_p^2}{a M_T \omega_b^2}, \quad l_b = a + \frac{J_T \omega_p \varsigma_b}{a M_T \omega_b \varsigma_b}. \tag{19}$$

Setting Δ to equal 0, 0.05 and 0.1, and using Eqs. (17)–(19) results in the parameter values shown in Table 2. The undamped natural frequencies calculated from the linearized model are shown in Table 3, and the corresponding mode shapes for $\Delta = 0.10$ m are shown in Fig. 11.

From these results, it is apparent that changing the locations of k_3, and k_4, and adjusting the parameters to agree with the subsystem modelling, does not have a noticeable effect on the natural frequencies of the full system. Although the undamped natural frequencies do not match the experimentally measured resonance frequencies, mode 3 is similar in shape to the deflections of the mannequin observed in experiments when excited at 5.5 Hz, and mode 4 is similar to the deflections of the mannequin at 7.5 Hz. Thus, later results will also use parameter values for $\Delta = 0.10$ m.

4.2. The effect of changing k_2 in the model

The stiffness k_2 was initially not included in the model because the mannequin did not contact the seat back. However, its exclusion limits the types of motions possible for the torso of the mannequin, and results in the presence of a very low-frequency mode, not observed in the experiment. It was therefore decided to explore the effect of including k_2. The results of the linear modal analysis are shown in Table 4 and Fig. 12.

Inclusion of k_2 introduces a new fore-and-aft mode (mode five in Table 4), and this is the mode most affected by variations in k_2, its associated natural frequency increasing as k_2 increases. The natural frequency of the up-and-down mode of vibration (mode four in Table 4), is initially

Table 2
Stiffness, damping and location parameters as a function of Δ

Δ (m)	l_a (m)	k_3 (N/m)	k_4 (N/m)	l_b (m)	c_3 (N s/m)	c_4 (N s/m)
0	0.174	16,239	64,548	0.2729	151.38	157.16
0.05	0.1476	30,722	50,065	0.2981	216.42	92.11
0.1	0.1636	61,532	19,254	0.5162	285.23	23.31

Table 3
Natural frequencies in Hertz as a function of Δ

Mode	1	2	3	4	5	6
$\Delta = 0.00$	$< 1.0 \times 10^{-7}$	1.92	4.46	5.97	8.91	15.44
$\Delta = 0.05$	$< 1.0 \times 10^{-7}$	1.97	4.46	5.96	8.93	15.44
$\Delta = 0.10$	$< 1.0 \times 10^{-7}$	1.92	4.46	5.97	8.91	15.44

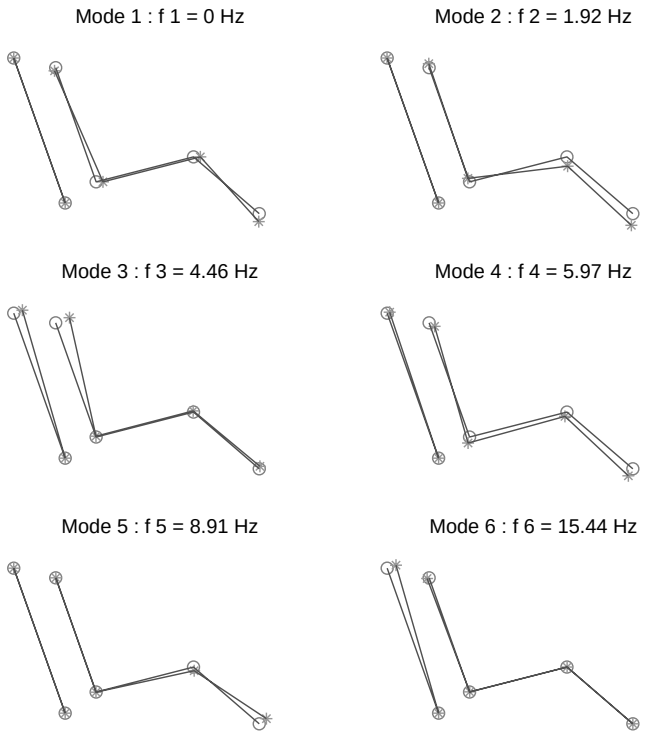

Fig. 11. Mode shapes of the headless mannequin motion for $\Delta = 0.10$ m. The first mode shape is a rigid body motion.

Table 4
Natural frequencies in Hertz as a function of changing k_2 ($k_1 = 23,059$ N/m)

Mode	$k_2 = 0.0$	$k_2 = 1.0 \times k_1$	$k_2 = 5.0 \times k_1$	$k_2 = 8.0 \times k_1$	$k_2 = 12.0 \times k_1$	$k_2 = 16.0 \times k_1$
1	0	—	—	—	—	—
2	1.92	1.88	1.89	1.89	1.89	1.89
3	4.46	4.52	4.37	4.39	4.39	4.39
4	6.97	6.30	5.23	5.34	5.39	5.41
5	—	3.44	9.48	11.38	13.06	13.88
6	8.91	8.91	8.81	8.88	8.89	8.89
7	15.44	15.48	15.74	16.08	16.95	18.31

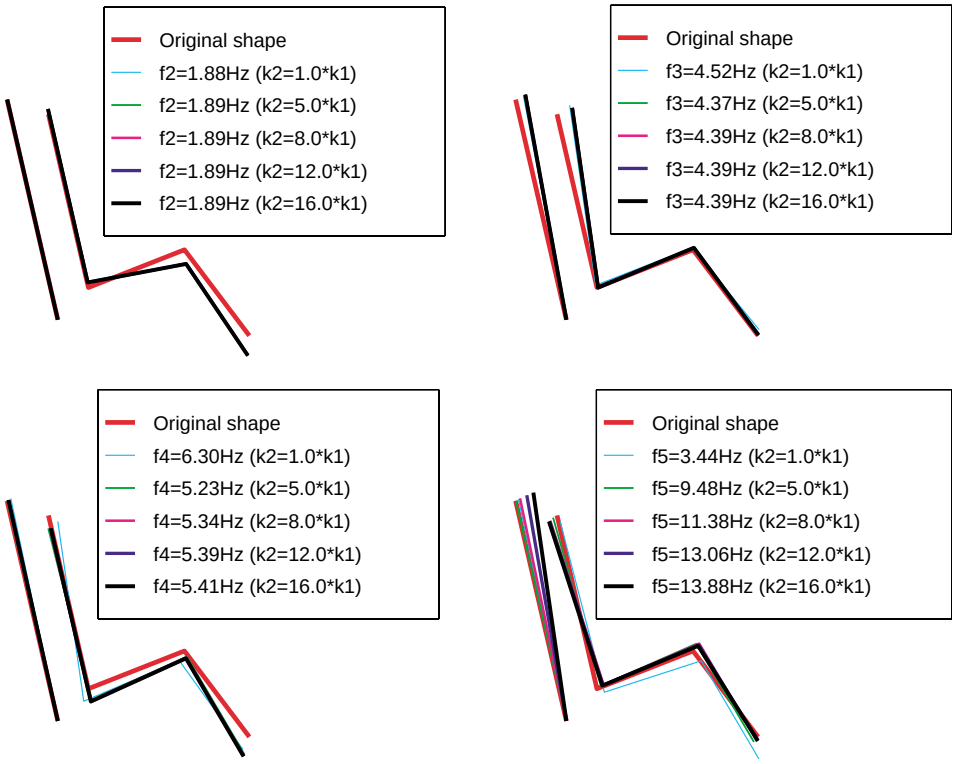

Fig. 12. The effect on the second, third, fourth and fifth mode shapes of the mannequin due to changes in the stiffness of spring k_2. Shown are $k_2 = \{0, 1, 5, 8, 12, \text{and} 16\} \times k_1$.

reduced by the inclusion of k_2 and then gradually increases as k_2 increases beyond 5 times k_1. Mode 7 is the only other mode significantly affected by the inclusion of k_2. In Fig. 12 the variation in four of the mode shapes as the stiffness k_2 is changed is shown. Clearly, the shape of mode 5 is the most affected, as is the corresponding frequency (Table 4).

4.3. *Effect of changing* k_1

The effects of varying values of k_1 on the natural frequencies of the system are shown in Table 5. In this model k_2 is set to be 12 times the baseline value of k_1. The most significant changes in natural frequencies occur for modes five (fore–aft horizontal motion), and seven (predominantly a seat back motion), with a smaller, but significant, change in the natural frequency of mode three (seat back and torso rotation). Very interestingly, the natural frequencies of modes that comprise mainly of up-and-down motion (modes two and four), and the natural frequency of mode six involving predominantly knee motion are barely affected by these changes. These mode shapes, not shown, only vary in terms of the amplitude as k_1 varies; the basic shapes do not change. The modal amplitudes most affected are those of the third and fifth modes.

Table 5
Natural frequencies in Hertz as a function of changing k_1. The baseline value of k_1 is 23,059 N/m

Mode	$k_1' = 0.5 \times k_1$	$k_1' = 0.75 \times k_1$	$k_1' = 1.0 \times k_1$	$k_1' = 2.0 \times k_1$	$k_1' = 4.0 \times k_1$
2	1.89	1.89	1.89	1.89	1.89
3	3.74	4.15	4.39	4.83	5.07
4	5.39	5.39	5.39	5.39	5.40
5	11.60	12.45	13.06	14.00	14.33
6	8.89	8.89	8.89	8.89	8.89
7	15.84	16.31	16.95	20.33	26.69

Table 6
Natural frequencies in Hertz as a function of changing k_3 and k_4. The baseline values ($\Delta = 0.10$ m) are: $k_3 = 61,532.0$ N/m and $k_4 = 19,254$ N/m

Mode	$0.1 \times (k_3, k_4)$	$0.5 \times (k_3, k_4)$	$1.0 \times (k_3, k_4)$	$2.0 \times (k_3, k_4)$	$4.0 \times (k_3, k_4)$
2	0.60	1.34	1.89	2.64	3.64
3	4.39	4.40	4.39	4.40	4.42
4	1.78	3.91	5.39	7.03	10.83
5	12.87	12.95	13.06	13.38	14.54
6	8.58	8.70	8.89	9.47	8.10
7	16.92	16.93	16.95	17.00	17.20

4.4. *Effect of changing k_3 and k_4*

4.4.1. *Changing springs three and four simultaneously*

Next, the effects of changing k_3 and k_4 were explored. The natural frequencies and the corresponding mode shapes are shown in Table 6 and in Fig. 13, respectively. In the model the value of k_2 was set at 12 times the baseline value for k_1. As k_3 and k_4 increase together, the natural frequencies of modes two (vertical motion of knee), and four (vertical motion of torso) increase. Also, the natural frequencies of modes five, six and seven increase slightly. Mode shape 4 is most affected by the changes. As can be seen in Fig. 13, although the frequency of mode 2 increases sixfold the mode shape changes are very small compared to those for mode 4.

4.4.2. *Effects of changing k_3, and k_4 individually*

The effects on the natural frequencies from changing k_3 alone are shown in Table 7, and those from changing k_4 are shown in Table 8. Mode shape 3 (seat back and torso rotation), as shown in Fig. 14, changes little but mode shape 4 (up and down motion) changes particularly in the leg motion. Again the natural frequencies most strongly affected are those associated with the vertical vibrations, that is modes two and four. The natural frequency of mode four is more sensitive to changes in k_3 than to changes in k_4; this is not unexpected as spring three is located at the mannequin's bottom, a major contact area between the seat and the mannequin. The opposite is

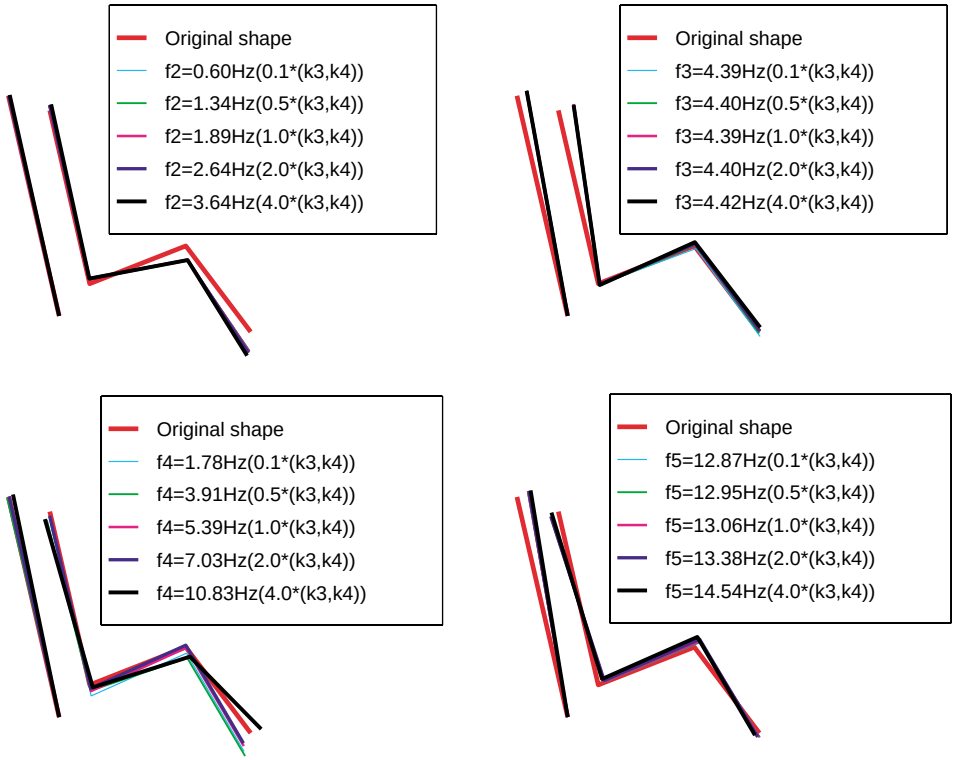

Fig. 13. The effect on the second, third, fourth and fifth mode shapes of proportional changes in the stiffnesses k_3 and k_4. Changes shown are $\{0.1, 0.5, 1.0, 2.0, \text{and } 4.0\} \times$ baseline values of k_3 and k_4.

Table 7
Natural frequencies in Hertz as a function of changing k_3. Baseline values ($\Delta = 0.10$ m): $k_3 = 61,532.0$ N/m and $k_4 = 19,254$ N/m

Mode	$0.5 \times (k_3)$	$0.75 \times (k_3)$	$1.0 \times (k_3)$	$2.0 \times (k_3)$	$4.0 \times (k_3)$
2	1.70	1.82	1.89	2.00	2.05
3	4.40	4.39	4.39	4.39	4.39
4	4.30	4.88	5.39	6.91	10.15
5	12.98	13.02	13.06	13.27	13.95
6	8.82	8.85	8.89	9.12	8.08
7	16.94	16.94	16.95	16.98	17.07

true for mode two (vertical knee motion), where k_4 appears to play a stronger role. Again, spring 4 is located close to the knee and hence this result is expected. The natural frequency of mode six (predominantly knee motion) is affected nearly equally by changes in k_3 or k_4.

It is interesting to note that when Δ was varied, the values of k_3 and k_4 varied considerably, see Table 2. However, the variation in that case was done while preserving the frequencies

Table 8
Natural frequencies in Hertz as a function of changing k_4. Baseline values ($\Delta = 0.10$ m) are $k_3 = 61,532.0$ N/m and $k_4 = 19,254$ N/m

Mode	$0.5 \times (k_4)$	$0.75 \times (k_4)$	$1.0 \times (k_4)$	$2.0 \times (k_4)$	$4.0 \times (k_4)$
2	1.42	1.69	1.89	2.38	2.79
3	4.39	4.39	4.39	4.40	4.40
4	5.17	5.28	5.39	5.79	6.37
5	13.02	13.04	13.06	13.15	13.39
6	8.75	8.82	8.89	9.19	9.88
7	16.94	16.95	16.95	16.97	17.00

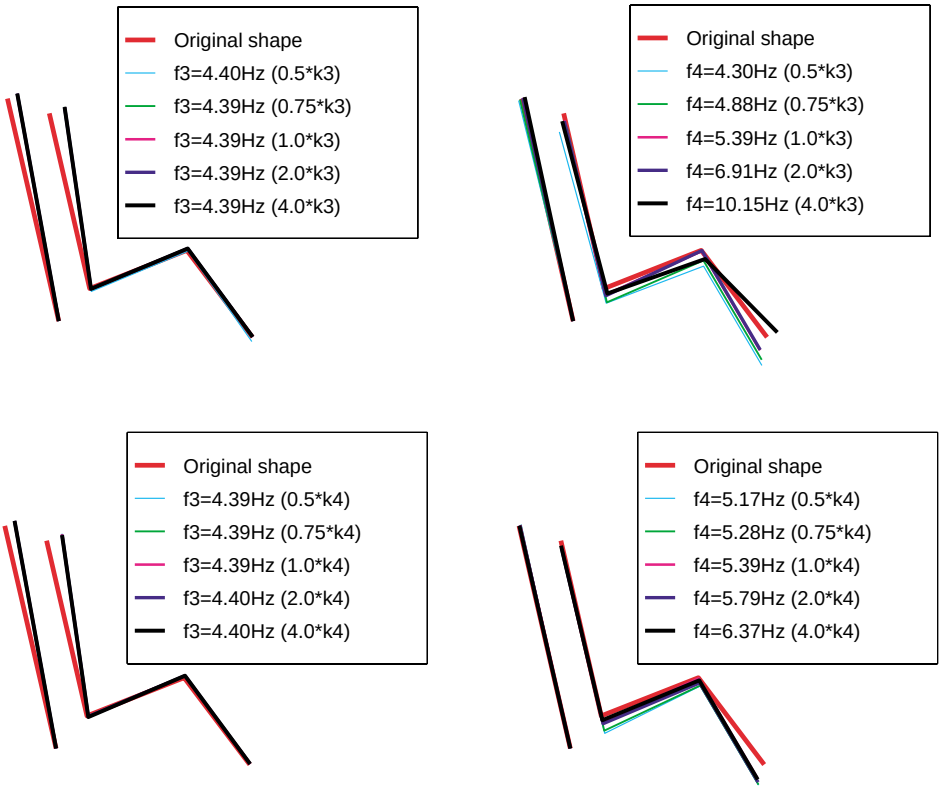

Fig. 14. Effects of stiffnesses k_3 and k_4 on the third and second mode shapes: (a) and (b) variations in the stiffness k_3; (c) and (d) variations in the stiffness k_4. In each case $\{0.5, 0.75, 1.0, 2.0, \text{and } 4.0\} \times$ baseline values are shown. Baseline values ($\Delta = 0.10$ m) are $k_3 = 61,532.0$ N/m and $k_4 = 19,254$ N/m.

of the pitching and bounce modes of the hips-and-thighs on the seat cushion subsystem. If k_3 and k_4 are varied independently, the natural frequencies of the subsystem will not necessarily be preserved, and thus the natural frequencies and modes shapes of the whole system will also change.

4.5. Effect of varying k_s

The value of the seat back torsional stiffness k_s estimated from the experiment is 7,194.94 N/rad. The changes in natural frequencies when k_s is varied are shown in Table 9. Again, beyond changes in amplitudes of response, the mode shapes do not change substantially with changing k_s, although the "synchronization" of the torso and the seat back rotation is affected, in that their amplitudes of motion are not changed equally when k_s is changed. The natural frequencies of the third mode (seat back torso rotation) and the seventh mode (seat back rotation alone) are the only ones strongly affected by changes in k_s, and they increase as k_s is increased.

4.6. Effects of changing linear and torsional damping values (c_i and $\boldsymbol{T}_i$)

First, the effect of changing all the linear and torsional damping coefficients by the same factors was examined. This was followed by a study on the effect of changing the damping terms individually. The coefficients of the friction moments will be denoted by $\boldsymbol{T}_i$ N m s/rad and, from Eq. (7), are equal to 2 $T_{max,i}/\omega_{i,0}$ where $\omega_{i,0} = 0.349$ rad/s [20]. The frequency response magnitudes are plotted from 0 to 10 Hz. In this range the second, third, fourth and sixth modes have undamped natural frequencies at 1.89, 4.39, 5.39 and 8.89 Hz, respectively. For mode numbering refer to Table 4, columns 1 and 6. As will be seen in the following results, damping and the friction in the joints have a strong influence on the number and location of the resonance peaks in the spectrum. The complexities of the model make it difficult to apply simplistic explanations such as "more damping will result in lower resonant frequencies and peaks".

4.6.1. Changing the linear and torsional damping coefficients simultaneously

In order to explore the effects of changing the coefficients of each of the viscous dampers, c_1 to c_5, and the coefficients of the friction moments at the joints, $\boldsymbol{T}_2$ and $\boldsymbol{T}_3$, Eq. (11) were used to evaluate the frequency response functions. The stiffness and damping values used in analysis are shown in Tables 1 and 2, with the exception that k_2 is set to 12 k_1, and these values correspond to the case where $\Delta = 0.1$ m. The joint friction coefficients used in this analysis were $\boldsymbol{T}_2 = 202.18$ N s/rad and $\boldsymbol{T}_3 = 80.87$ N s/rad. The frequency response magnitudes as a function of c_i and $\boldsymbol{T}_i$ are shown in Figs. 15 and 16, respectively. The dark solid lines indicate the frequency response magnitude of the baseline model ($\Delta = 0.10$ m).

Table 9
Natural frequencies in Hertz as a function of changing k_s. The baseline value of k_s is 7194.94 N/rad

Mode	$0.1 \times (k_s)$	$0.5 \times (k_s)$	$1.0 \times (k_s)$	$2.0 \times (k_s)$	$4.0 \times (k_s)$
2	1.92	1.89	1.89	1.89	1.89
3	1.64	3.42	4.39	5.23	5.98
4	5.38	5.38	5.39	5.45	5.36
5	12.00	12.58	13.06	13.50	13.76
6	8.89	8.89	8.89	8.89	8.89
7	15.41	15.99	16.95	19.24	23.71

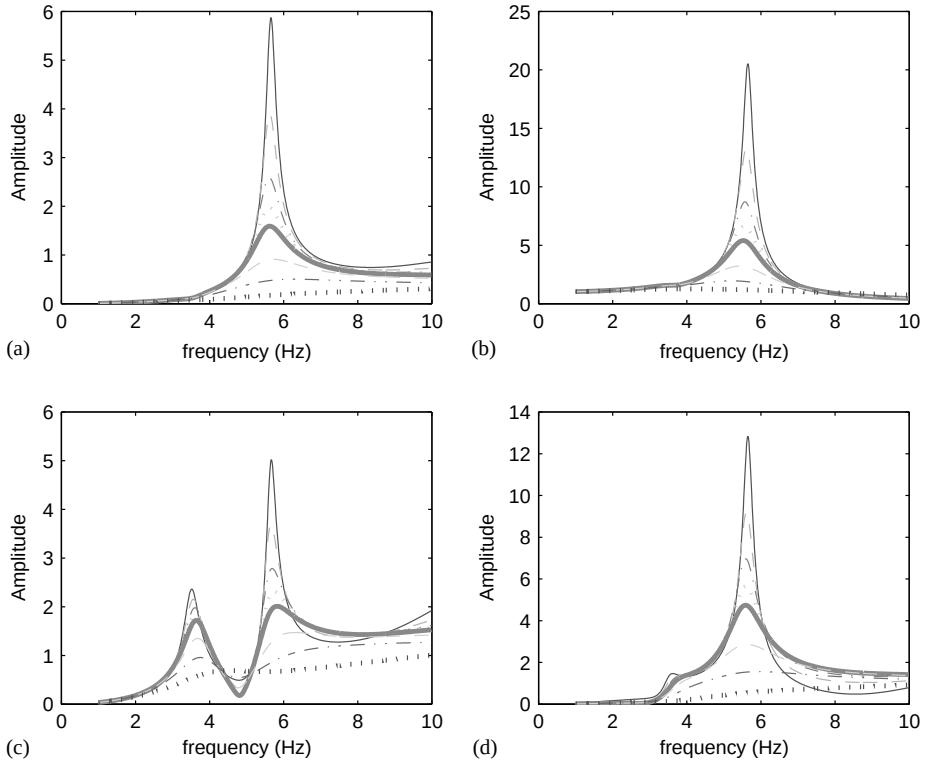

Fig. 15. The effect of varying viscous damping parameters: $c_i = (0.1, 0.25, 0.5, 0.75, 1.0, 2.0, 4.0, 10.0) \times$ baseline c_i, $i = 1, 3, 4, 5$, on frequency response function magnitudes relating (a) horizontal acceleration, (b) vertical acceleration, (c) angular acceleration at the hip joint, and (d) angular acceleration at the knee joint, to base acceleration. Graph lines corresponding to the various scalings of c_i are: thin solid (0.1), dashed (0.25), dash–dot (0.5), light dotted (0.75), dark solid (baseline), light dashed (2.0), dash–dash–dot (4.0), dark dotted (10.0).

The results shown in Fig. 15 are classic illustrations of the effect of damping on resonant behaviour of dynamic systems. As the viscous damping ratios increase, the peak magnitudes in the frequency response plots decrease. The results shown in Fig. 16 are surprising because an increase in the torsional damping, at higher damping values, leads to an increase in the location of the resonant natural frequency, and also to an increase in amplitude. This is most clearly illustrated in Figs. 16(b) and (c). This result is a little surprising and may be attributable to a "locking" of the joints, causing an effective reduction in the number of degrees of freedom in the mannequin motion. This phenomenon will be explored further in Section 4.6.3. At lower levels of joint damping, the increase in damping follows the expected trends: lowering of resonant amplitude and decrease in natural frequency, similar to the trends shown in Fig. 15 when the c_i were increased.

4.6.2. Effect of changing individual linear damping constants c_1, c_3, c_4 and c_5

In Fig. 17, the magnitudes of the frequency response functions between the base excitation and the hip joint vertical vibration are shown. In parts (a) through (d), c_1, c_2, c_3 and c_4 are, respectively, varied individually.

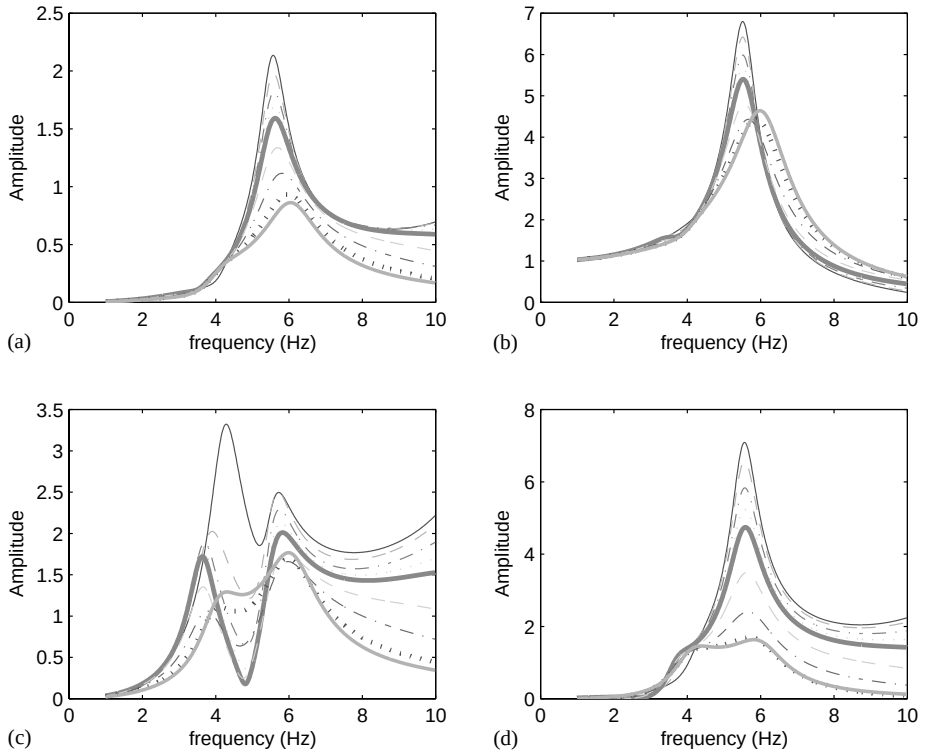

Fig. 16. The effect of varying joint damping coefficients: $\boldsymbol{T}_i = (0.1, 0.25, 0.5, 0.75, 1.0, 2.0, 4.0, 10.0, 20.0) \times$ baseline $\boldsymbol{T}_i$, $i = 2, 3$, on the frequency response magnitudes relating: (a) horizontal acceleration, (b) vertical acceleration, (c) angular acceleration at the hip joint and (d) angular acceleration at the knee joint to base acceleration. Graph lines corresponding to the various scalings of $\boldsymbol{T}_i$ are: thin solid (0.1), dashed (0.25), dash–dot (0.5), light dotted (0.75), dark solid (baseline), light dashed (2.0), dash–dash–dot (4.0), dark dotted (10.0), thin dark solid (20.0).

It can be seen from the results that c_3 has the strongest effect on the rail to seat bottom vertical frequency response function. The main peak corresponds to a motion similar to that of mode four (up and down sliding along the seat back). The smaller peak appears to be related to the seat back and torso rotational mode (mode three). These modes of response were confirmed by calculating the operating deflection shapes of the model at these two peak frequencies. Since c_3 is the closest damper to the hip joint, it is not surprising that it has the strongest influence on the "up-and-down" mode of vibration.

4.6.3. Effect of changing friction moment constants $\boldsymbol{T}_2$ and $\boldsymbol{T}_3$ individually

The effect of changing the friction moments at the joints was also explored and the corresponding frequency response functions relating the hip joint motion to the base motion are shown in Fig. 18. The baseline values are taken from Nishiyama [20,21], and are supposed to be those for a human, not a mannequin. No description of how they were calculated is given. These parameters are difficult to measure and hence Nishyama's data was used as a starting point.

The friction coefficient at the knee joint ($\boldsymbol{T}_3$) has a much greater effect on the frequency response than the friction coefficient at hip joint ($\boldsymbol{T}_2$). When $\boldsymbol{T}_2$ is equal to or larger than its

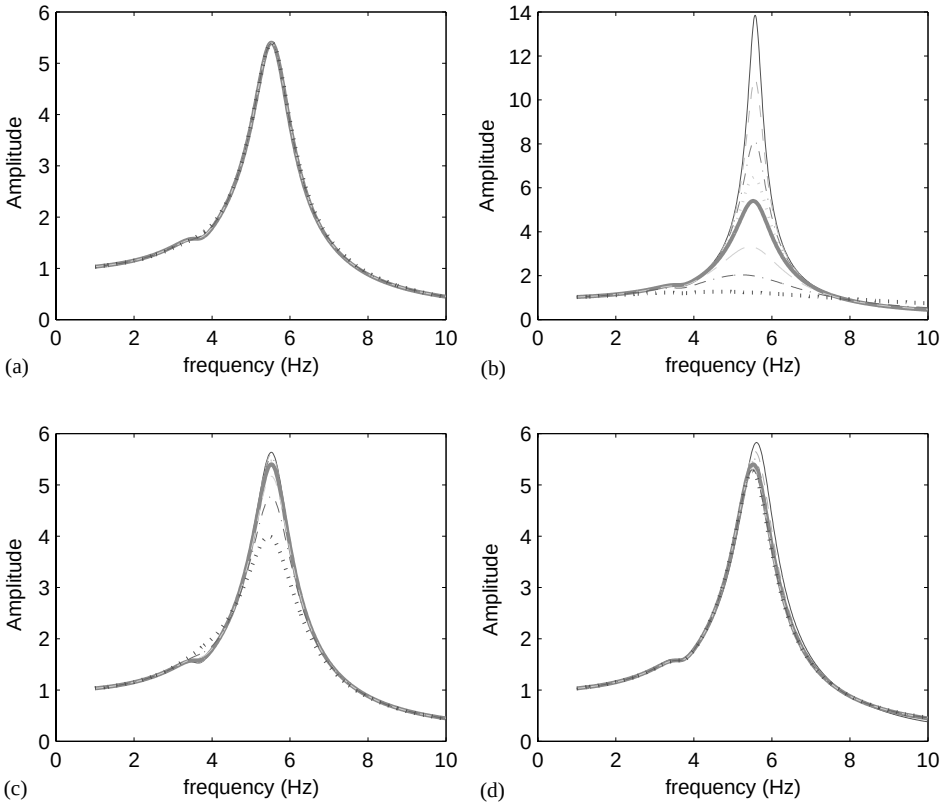

Fig. 17. Frequency response function magnitude, relating vertical acceleration of the hip joint to base acceleration, as a function of changing damping values: $c_i = (0.1, 0.25, 0.5, 0.75, 1.0, 2.0, 4.0, 10.0) \times$ (baseline c_i). (a) c_1 varies, (b) c_2 varies, (c) c_3 varies, and (d) c_4 varies. Graph line types corresponding to the various scalings of c_i are: thin solid (0.1), dashed (0.25), dash–dot (0.5), dotted (0.75), dark solid (baseline), light dashed (2.0), dash–dash–dot (4.0), dark dotted (10.0).

baseline value (202.18 N s/rad), increases in $\boldsymbol{T}_3$ lead to increases in the frequency at which the peak occurs in the frequency response function, as shown in Figs. 18(c) and (d). However, when $\boldsymbol{T}_2$ is smaller than its baseline value, as $\boldsymbol{T}_3$ increases the peak occurs at a slightly lower frequency, as shown in Fig. 18(b). As both $\boldsymbol{T}_2$ and $\boldsymbol{T}_3$ increase, the smaller resonant peak in the frequency response close to 3.64 Hz becomes insignificant.

5. Matching the experiment and simulation

As discussed earlier, the two main resonance frequencies of the headless mannequin measured in experiments are at 5.5 and 7.5 Hz. The deflection shape at 5.5 Hz is mostly a seat back and torso in-phase rotation, and the deflection shape at 7.5 Hz is mostly up-and-down motion of the hip joint with the torso sliding up and down the seat. In Fig. 12, the analysis of the system with the parameters set at the results of the subsystem modelling is shown for varying values of k_2. The experimental deflection shapes are similar to the predicted mode shapes when k_2 was set to $12k_1$.

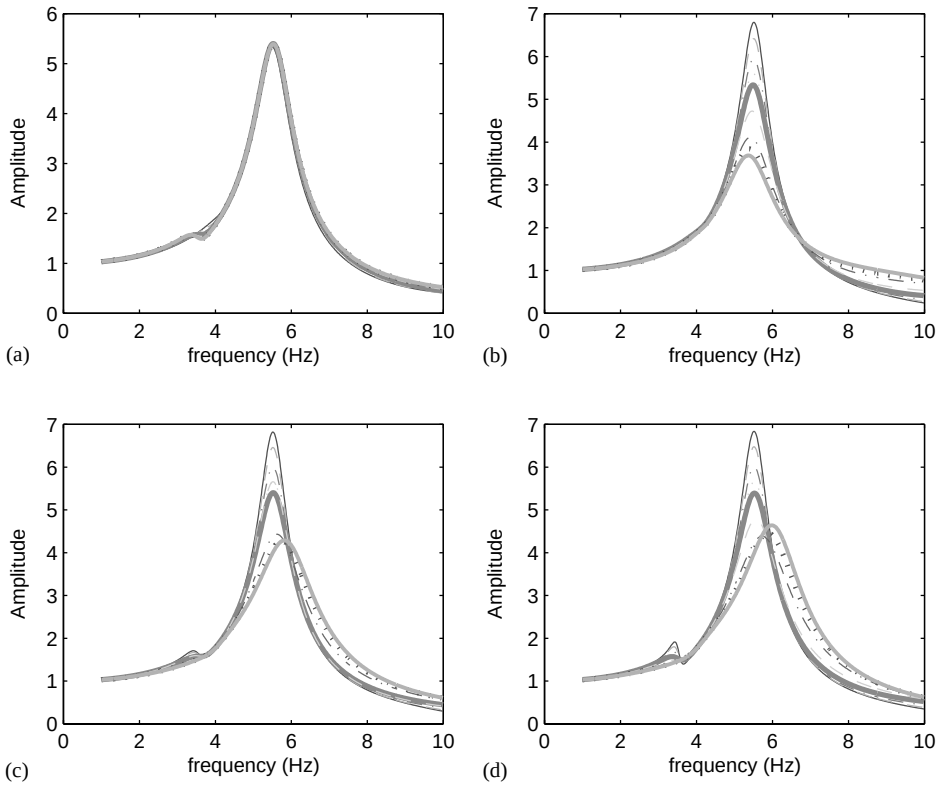

Fig. 18. The effect of changing joint friction moment coefficients: $\boldsymbol{T}_i = (0.1, 0.25, 0.5, 0.75, 1.0, 2.0, 5.0, 10.0, 20.0) \times$ baseline $\boldsymbol{T}_i$, on frequency response magnitudes relating vertical acceleration of the hip joint to base acceleration: (a) $\boldsymbol{T}_2$ varies and $\boldsymbol{T}_3 = 80.87\,\mathrm{N\,m\,s/rad}$, (b) $\boldsymbol{T}_3$ varies and $\boldsymbol{T}_2 = 20.22\,\mathrm{N\,m\,s/rad}$, (c) $\boldsymbol{T}_3$ varies and $\boldsymbol{T}_2 = 202.18\,\mathrm{N\,m\,s/rad}$, and (d) $\boldsymbol{T}_3$ varies and $\boldsymbol{T}_2 = 4043.54\,\mathrm{N\,m\,s/rad}$. Graph lines corresponding to the various scalings of $\boldsymbol{T}_i$ are: thin solid (0.1), dashed (0.25), dash–dot (0.5), light dotted (0.75), dark solid (baseline), light dashed (2.0), dash–dash–dot (5.0), dark dotted (10.0), thin dark solid (20.0).

However, neither the third and the fourth undamped natural frequencies ($f_3 = 4.39\,\mathrm{Hz}$ and $f_4 = 5.39\,\mathrm{Hz}$, respectively) nor the resonance locations (3.64 and 5.53 Hz) in the model's frequency response functions (Fig. 16) correspond to the resonance frequencies observed in the experiment.

In order to match the experiment and simulation, the resonance (peak response) frequencies need to be increased. Based on the results of the parameter variation studies, several guidelines for matching the observed and predicted frequency response functions were identified.

- To increase the resonance frequency of the up-and-down motion (mode 4) from 5.53 Hz in simulation to the 7.5 Hz observed in experiment, values of k_3 and k_4 could be increased (Tables 6–8). Also, $\boldsymbol{T}_3$ could also be increased above 4 times its baseline value (Figs. 16 and 18). The most significant effects will come from increasing k_3 (Table 7).
- Since k_s has the strongest effect on seat back and torso mode (Table 9), the value of k_s could be increased to increase seat back and torso resonance from 3.64 Hz in the simulation to 5.5 Hz in the experiment. Increasing k_1 will also increase the undamped natural frequency associated

Table 10
New 'adjusted' stiffness and damping parameters for the system

Stiffness of each spring	Values (N/(m or rad))	Damping coefficient	Values (N s/m)	Friction moment	Values (N s/rad)
$k_1' = 2.65 \times k_1$	61,106.4	$c_1' = 0.25 \times c_1$	17.62	$T_2' = 20 \times T_2$	4043.55
$k_2 = 12 \times k_1$	276,708.0	c_2	0.00	$T_3' = 1.5 \times T_3$	121.31
$k_3' = 2.05 \times k_3$	126,140.6	$c_3' = 2.1 \times c_3$	598.98		
$k_4' = 2.05 \times k_4$	39,470.7	$c_4' = 2.1 \times c_4$	48.95		
k_5	15,279.0	$c_5 = 20 \times c_1$	1409.6		
$k_s' = 3.0 \times k_s$	21,584.8				

with this motion (Table 5). Lowering $\boldsymbol{T}_2$ and $\boldsymbol{T}_3$ to below 0.25 times their baseline values will also increase the frequency location of this resonance in the spectrum (Fig. 16(c)).

- To reduce the amplitudes of up-and-down motion at resonance, c_3 and c_4 can be increased, as shown in Figs. 17(b) and (c). In certain regions $\boldsymbol{T}_2$ and $\boldsymbol{T}_3$ can be increased to reduce the amplitude, but in other regions an increase in these parameters can lead to an increase in the peak amplitude (Figs. 16(b) and (c)).
- To increase the amplitudes of the seat back torso resonance, c_3 and c_4 can be decreased. Reducing $\boldsymbol{T}_2$ and $\boldsymbol{T}_3$ can lead to dramatic increases in amplitude, and increasing $\boldsymbol{T}_2$ and $\boldsymbol{T}_3$ well above their baseline values can also lead to an increased resonance amplitude (Figs. 16(b) and (c)).
- By using these guidelines, a new set of values was found for the stiffness and damping parameters, and also for the torsional dampers at the joints. These ratios and values are shown in Table 10. The undamped natural frequencies and the corresponding mode shapes from the linear modal analysis are shown in Fig. 19.

By using these parameters, good agreement was obtained between the model frequency response and the measured frequency response, as shown in Fig. 20. The solid line is the estimate generated from measurements. Below 5 Hz the measurements were noisy due to low energy excitation into the system at these frequencies. The signal-to-noise ratios are progressively worse as the frequency approaches 0 Hz. Since the H1 frequency response function estimate was used [34], at low signal-to-noise ratios of the input, the frequency response function magnitude will be biased towards zero, and will approach zero as the signal to noise ratio becomes very small, which was the case here at very low frequencies. Thus, frequency response estimates below 3 Hz are very poor and are not plotted. The lighter line is the frequency response derived from the linear analysis (Eq. (10)). The crosses, which lie on the top of the lighter line, are the results of performing a full non-linear dynamic analysis (Eq. (3)) of the system responding to a random input, similar to that used in the experiment, and then generating the H1 frequency response estimate.

The characteristics of the input to the seat rails were as follows. First, the input was a base acceleration with a r.m.s. value of $0.006\,\mathrm{g\,m/s^2}$. Second, the frequency range of the input was 1–50 Hz. The input spectrum was shaped by using filters to approximate the actual input power spectral density measured on the shaker table. The total analysis time was just over 64 s with a

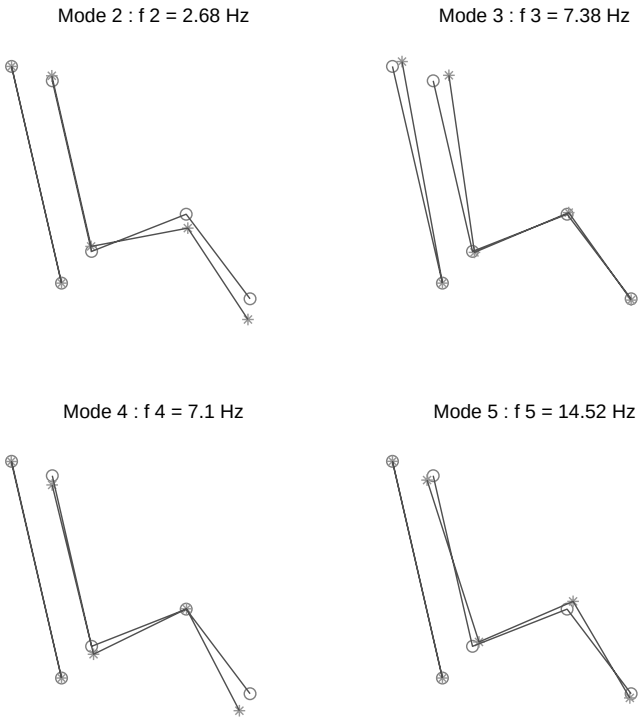

Fig. 19. The undamped natural frequencies and corresponding mode shapes for four of the modes derived from the model with parameters as shown in Table 10.

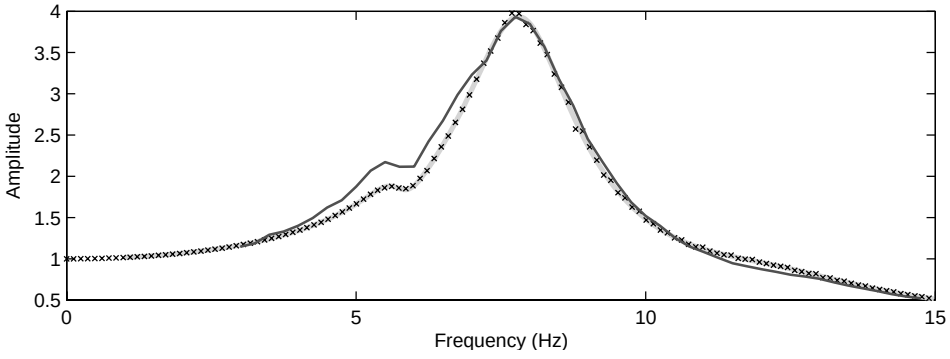

Fig. 20. Frequency responses relating vertical acceleration ($\ddot{\zeta} + \ddot{z}$) of hip joint to base acceleration ($\ddot{z}$). Dark solid line: experimental results, light solid line: linear model frequency response function, line with crosses: estimate from simulation using full non-linear dynamic analysis.

sample rate of 2048 samples per second. In the spectral density calculations, the data was split into 50% overlapping, 4 s segments, and windowed with a Hann window.

From the results one can conclude that the linearization produces an accurate model at these input levels. The up-and-down resonance at 7.5 Hz is well predicted by the model. There is some

mismatch at the lower seat back torso resonance at 5.5 Hz. Some of these differences could be explained from the measurements where perhaps some of the rotational motion, in addition to vertical motion, was being picked up by the accelerometer on the mannequin's bottom. Because of the large influence of the torsional damping coefficients on the resonance (peak response) location, the operating deflection shapes were generated at the two resonance frequencies, rather than relying on a modal analysis of the undamped system. These are shown in Fig. 21. These agree well with those observed in the experiment (Fig. 5).

The main resonance of the seat–mannequin system was at a higher frequency than is typically found with humans occupying car seats. It was of interest to see if by modifying the mannequin characteristics to more closely match that of a human whether it was possible to shift the resonance of the system significantly. The data for a 50th percentile male are shown in Table A.1 [36]. The frequency response function magnitudes shown in Fig. 22 are for the seat–mannequin system and for a seat–50th percentile male system. The mass moments of inertia were based on the mannequin but scaled to take into account the mass difference between the mannequin and the 50th percentile male. The dimensions of the 50th percentile male model were adjusted to be the same as the mannequin. It is known that different weight distributions will produce different compressions in the foam which will affect the stiffness, and foam is much stiffer at low ($<10\%$)

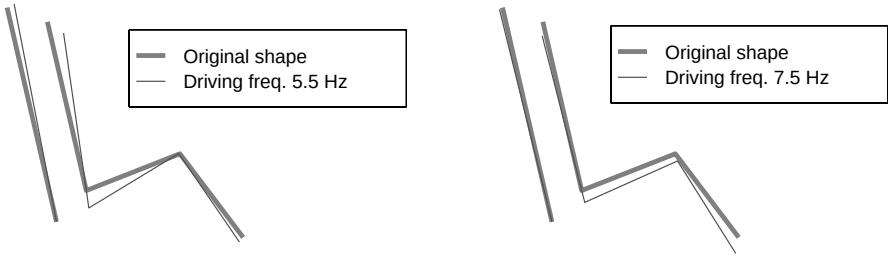

Fig. 21. Operating deflection shapes predicted by the linearized analytical model at the two main resonance (peak response) locations: (a) 5.5 Hz, and (b) 7.5 Hz. Model parameters are shown in Table 10.

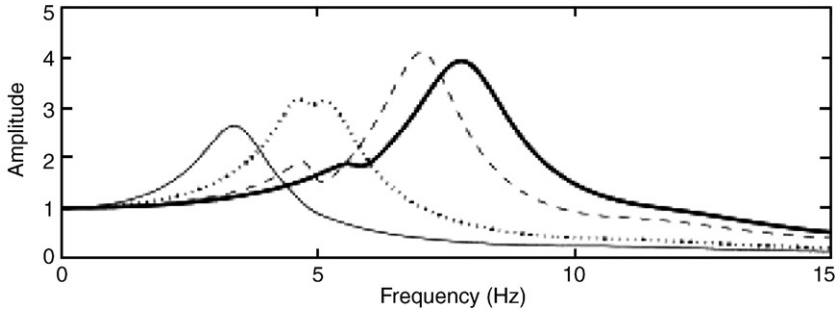

Fig. 22. Frequency responses relating vertical acceleration of hip joint to base acceleration of a seat–mannequin and a seat–50th percentile male system. Dark solid line: seat–mannequin system, dashed line: seat–50th percentile male system, dotted line: seat–50th percentile male system with k_3 and k_4 reduced by half, light solid line: seat–50th percentile male system with k_4 reduced by half and $k_3 = k_4$.

and very high (> 50%) compression levels than it is at medium levels of compression. With some foams the stiffness in the middle range can be very low. The three plots associated with the 50th percentile male are for three settings of the stiffnesses that represent the effect of the seat cushion (k_3 and k_4). Clearly, it can be seen that both the mass distribution and the seat stiffness play a large role in where the resonances occur and also the strength and relationship of the two peaks in this part of the frequency response. This figure clearly illustrates that two-dimensional models with this level of complexity are capable of predicting the types of frequency response behaviour observed in experiments with both mannequins and humans.

6. Summary and conclusions

A simplified two-dimensional modelling approach for occupied car seats was demonstrated to be feasible. The model consisted of interconnected masses, springs and dampers. Because foam is a highly non-linear material and the stiffness and damping properties are dependent on compression level, the mannequin–seat system was initially broken down into subsystems and experiments conducted to determine approximate values for model parameters. A short study of the effect of changing model parameters on natural frequencies, mode shapes and resonance locations in frequency response functions was described, highlighting the influence of particular model parameters on features in the mannequin's vibration response. Good agreement between experimental and simulation frequency response estimates was obtained both in terms of locations of resonances and system deflection shapes at resonance, indicating that this is a feasible method of modelling seated occupants.

The subsystem modelling is an important step to finding approximate values for the parameters in the model. While this was performed for a specific mannequin–seat system, the approach is sufficiently general to be applicable to other seat–mannequin systems. Reproducing the static deformation of the foam prior to the dynamic testing is important as the stiffness is strongly dependent on compression level. The subsystem modelling did not include estimation of the torsional damping in the mannequin's joints. The model response was sensitive to the torsional damping in the joints, and therefore methods to estimate these parameters experimentally should be established. Most of the model parameters had to be changed from the subsystem model predictions to produce good agreement with the experimentally determined frequency response function. The parameter tuning was done by using the parameter study results to guide the choice of parameters to effect the modification of a particular frequency response feature. While this extensive exploration gave much insight into the influence of model parameters, it would be desirable to automate this procedure, using the subsystem parameter estimates as the starting point.

Whether the deficiency in the subsystem-based model predictions is due to the influence of addition parameters in the full system that are unaccounted for in the model, e.g., surface friction and shearing of the foam as the mannequin slides along the seat back, or is due to deficient subsystem modelling needs to be investigated. The foam modelling is certainly deficient because it is well known that foam is a viscoelastic material. The influence of viscoelastic behaviour has been observed in experiments on car-seat foam conducted by the authors [11,17]. One extension of the seat model would be the inclusion of discrete viscoelastic elements. It is important to know whether it is essential to model these additional effects explicitly. Certainly, how their presence

affects component parameters in the model should be evaluated and will be addressed in future research. Currently research is also underway to develop similar models with non-linear springs, surface friction effects and viscoelastic elements, that predicts the static settling point, a necessary step to aid in the subsystem modelling stage in this dynamic model approach. Understanding these issues is essential to developing links between fundamental material properties and seat–mannequin model parameters, one step in the optimization of seat design for vibration comfort.

Acknowledgements

The authors wish to express their gratitude to Don Showers and Paul Leidtke at Johnson Controls for their support, both financial and intellectual. Without their support, this research would not have been possible. The support of Ken Karpczuk and Kuntal Thakurta of the Automotive Seating Group of Johnson Controls, who contributed their expertise in seat design and manufacturing issues, is also greatly appreciated. The authors also appreciate the efficiency of Beth Rogers from the Human Systems Information Analysis Center (HSIAC) and Sashi Kuppa of the National Highway Traffic Safety Administration (NHSTA) who helped us locate some of the reference material. Finally, we must acknowledge Rajani Ippili, a Mechanical Engineering graduate student at Purdue University, for his careful and painstaking checking of the models and the analysis.

Appendix A. Seat–mannequin system model parameters

The parameters of geometric dimensions, masses, and mass moments of inertia, are given in Table A.1.

Appendix B. Formulae for calculating the parameters in the non-linear model

Following is a list of the formulae used in the calculation of the elastic and damping terms on the right-hand side of the Eq. (8).

$$A_5: \quad \Delta(\xi) = \sum_{i=1}^{5} k_i \delta_i \frac{\partial \delta_i}{\partial \xi} + \sum_{i=1}^{5} c_i \dot{\delta}_i \frac{\partial \dot{\delta}_i}{\partial \dot{\xi}}, \qquad B_5: \quad \Delta(\zeta) = \sum_{i=1}^{5} k_i \delta_i \frac{\partial \delta_i}{\partial \zeta} + \sum_{i=1}^{5} c_i \dot{\delta}_i \frac{\partial \dot{\delta}_i}{\partial \dot{\zeta}},$$

$$D_4: \quad \Delta(\Theta_1) = \sum_{i=1}^{5} k_i \delta_i \frac{\partial \delta_i}{\partial \Theta_1} + \sum_{i=1}^{5} c_i \dot{\delta}_i \frac{\partial \dot{\delta}_i}{\partial \dot{\Theta}_1}, \qquad E_4: \quad \Delta(\Theta_2) = \sum_{i=1}^{5} k_i \delta_i \frac{\partial \delta_i}{\partial \Theta_2} + \sum_{i=1}^{5} c_i \dot{\delta}_i \frac{\partial \dot{\delta}_i}{\partial \dot{\Theta}_2},$$

$$G_4: \quad \Delta(\Theta_3) = \sum_{i=1}^{5} k_i \delta_i \frac{\partial \delta_i}{\partial \Theta_3} + \sum_{i=1}^{5} c_i \dot{\delta}_i \frac{\partial \dot{\delta}_i}{\partial \dot{\Theta}_3}, \qquad H_4: \quad \Delta(\Theta_4) = \sum_{i=1}^{5} k_i \delta_i \frac{\partial \delta_i}{\partial \Theta_4} + \sum_{i=1}^{5} c_i \dot{\delta}_i \frac{\partial \dot{\delta}_i}{\partial \dot{\Theta}_4},$$

$$S_2: \quad \Delta(\Theta_s) = \sum_{i=1}^{5} k_i \delta_i \frac{\partial \delta_i}{\partial \Theta_s} + \sum_{i=1}^{5} c_i \dot{\delta}_i \frac{\partial \dot{\delta}_i}{\partial \dot{\Theta}_s},$$

Table A.1
Parameter values for the seat–mannequin system and a 50% percentile male

Parameters	Seat–mannequin system used in experiments	50% percentile male
Mass of head (m)	3.988	4.536
Mass of torso, neck, pelvis and arms (m_2)	34.138	50.298
Mass of femur (m)	17.844	11.975
Mass of shin (m)	7.948	11.340
Total mass ($M_1 = m_1 + m_2 + m_3 + m_4$)	63.918	78.149
Mass moment of inertia of head (I_1)	0.02195	0.02497
Mass moment of inertia of torso, neck, pelvis and arms (I_2)	1.39277	2.05207
Mass moment of inertia of femur (I_3)	0.33520	0.22495
Mass moment of inertia of shin (I_4)	0.19732	0.28153
Length of head (l_1)	0.1207	0.1727
Length of torso and pelvis ($l_2 + l_3$)	0.6223	0.6248
Length of femur ($l_4 + l_5$)	0.5334	0.5283
Length of shin ($l_6 + l_7$)	0.4572	0.4927
Initial angle of head (Θ_{10})	100.0	100.0
Initial angle of torso (Θ_{20})	110.0	110.0
Initial angle of femur (Θ_{30})	14.0	14.0
Initial angle of shin (Θ_{40})	320.0	320.0
Angle of foot (β)	50.0	50.0
Angle of seat (Θ_{s0})	110.0	110.0
Distance from seat corner to base of foot rest (l_o)	0.9378	0.9378
Distance from the base of foot rest to heel (l_p)	0.1397	0.1397
Distance from seat rail to seat cushion (l_q)	0.163	0.163
Distance from seat back joint to position of k_1 (l_k)	0.578	0.578
Distance from seat back joint to position of k_2 (l_m)	0.076	0.076
Length of seat-back (l_l)	0.800	0.800
Z dir. initial position of hip joint (ζ_0)	0.110	0.110
X dir. initial position of hip joint (ξ_0)	0.165	0.165

Units: length (m), angle (degrees), mass (kg), mass moment of inertia (kg m^2).

where the definitions of the geometric parameters l_i, $i = 1, 2 \ldots 7$, $l_l, l_k, l_m, l_a, l_b, l_p, l_q$, and l_o, are given in Fig. 1, and the deflections δ_i, $i = 1, 2, 3, 4$ are defined below:

$$\delta_1 = \sqrt{f_1(\xi, \zeta, \Theta_2, \Theta_s)} - \delta_{10},$$

$$f_1 = \xi^2 + \zeta^2 + 2(l_k - l_m)\{\xi \cos\Theta_2 + \zeta \sin\Theta_2\} - 2l_k\{\xi \cos\Theta_s + \zeta \sin\Theta_s\}$$
$$- 2l_k(l_k - l_m)\{\cos\Theta_s \cos\Theta_2 + \sin\Theta_s \sin\Theta_2\} + l_k^2 + (l_k - l_m)^2,$$

$$\dot{f}_1 = \xi\dot{\xi} + \zeta\dot{\zeta} + (l_k - l_m)\{\dot{\xi} \cos\Theta_2 - \xi \sin\Theta_2 \cdot \dot{\Theta}_2 + \dot{\zeta} \sin\Theta_2 + \zeta \cos\Theta_2 \cdot \dot{\Theta}_2\}$$
$$- l_k\{\dot{\xi} \cos\Theta_s - \xi \sin\Theta_s \cdot \dot{\Theta}_s + \dot{\zeta} \sin\Theta_s + \zeta \cos\Theta_s \cdot \dot{\Theta}_s\} - l_k(l_k - l_m)$$
$$\times \{\cos\Theta_s \sin\Theta_2 \cdot \dot{\Theta}_s + \sin\Theta_s \cos\Theta_2 \cdot \dot{\Theta}_2 - \cos\Theta_s \sin\Theta_2 \cdot \dot{\Theta}_2 + \sin\Theta_s \cos\Theta_2 \cdot \dot{\Theta}_s\},$$

$$\delta_{10} = \big[\xi_0^2 + \zeta_0^2 + 2(l_k - l_m)\{\xi_0 \cos\Theta_{20} + \zeta_0 \sin\Theta_{20} - 2l_k \cos(\Theta_{20} - \Theta_{s0})\}$$
$$- 2l_k\{\xi_0 \cos\Theta_{s0} + \zeta_0 \sin\Theta_{s0}\} + l_k^2 + (l_k - l_m)^2\big]^{1/2},$$

$$\delta_2 = \sqrt{f_2(\xi, \zeta, \Theta_s)} - \delta_{20},$$
$$f_2 = \xi^2 + \zeta^2 - 2l_m\{\zeta \sin\Theta_s + \xi \cos\Theta_s\} + l_m^2,$$
$$\dot{f}_2 = \xi\dot{\xi} + \zeta\dot{\zeta} - l_m\big\{\dot{\xi} \cos\Theta_s - \xi \sin\Theta_s \cdot \dot{\Theta}_s + \dot{\zeta} \sin\Theta_s + \zeta \cos\Theta_s \cdot \dot{\Theta}_s\big\},$$
$$\delta_{20} = \big[\xi_0^2 + \zeta_0^2 - 2l_m\{\zeta_0 \sin\Theta_{s0} + \xi_0 \cos\Theta_{s0}\} + l_m^2\big]^{1/2},$$

$$\delta_3 = \sqrt{f_3(\xi, \zeta, \Theta_3)} - \delta_{30}, \quad l_\Delta = \frac{\Delta}{\cos\Theta_{30}},$$
$$f_3 = \xi^2 + \zeta^2 + 2l_\Delta\{\xi \cos\Theta_3 + \zeta \sin\Theta_3\} - 2(\Delta + \xi_0)\{\xi + l_\Delta \cos\Theta_3\} + l_\Delta^2 + (\Delta + \xi_0)^2,$$
$$\dot{f}_3 = \xi\dot{\xi} + \zeta\dot{\zeta} + l_\Delta\{\dot{\xi} \cos\Theta_3 - \xi \sin\Theta_3 \cdot \dot{\Theta}_3 + \dot{\zeta} \sin\Theta_3 + \zeta \cos\Theta_3 \cdot \dot{\Theta}_3\}$$
$$- (\Delta + \xi_0)\dot{\xi} + l_\Delta(\Delta + \xi_0)\sin\Theta_3 \cdot \dot{\Theta}_3,$$
$$\delta_{30} = [\zeta_0 + l_\Delta \sin\Theta_{30}],$$

$$\delta_{4k} = \sqrt{f_{4k}(\xi, \zeta, \Theta_3)} - \delta_{4k0}, \quad l_{n1} = \frac{l_a + \Delta}{\cos\Theta_{30}}, \quad l_{j1} = \xi_0 + \Delta + l_a,$$
$$f_{4k} = \xi^2 + \zeta^2 + 2l_{n1}\{\xi \cos\Theta_3 + \zeta \sin\Theta_3\} - 2l_{j1}(\xi - l_{n1} \cos\Theta_3) + l_{n1}^2 + l_{j1}^2,$$
$$\dot{f}_{4k} = \xi\dot{\xi} + \zeta\dot{\zeta} + l_{n1}\{\dot{\xi} \cos\Theta_3 - \xi \sin\Theta_3 \cdot \dot{\Theta}_3 + \dot{\zeta} \sin\Theta_3 + \zeta \cos\Theta_3 \cdot \dot{\Theta}_3\}$$
$$- l_{j1}(\dot{\xi} + l_{n1} \sin\Theta_3 \cdot \dot{\Theta}_3),$$
$$\delta_{4k0} = [(\xi_0 + l_{n1} \cos\Theta_{30} - l_{j1})^2 + (\zeta_0 + l_{n1} \sin\Theta_{30})]^{1/2},$$

$$\delta_{4c} = \sqrt{f_{4c}(\xi, \zeta, \Theta_3)} - \delta_{4c0}, \quad l_{n2} = \frac{l_b + \Delta}{\cos\Theta_{30}}, \quad l_{j2} = \xi_0 + \Delta + l_b,$$
$$f_{4c} = \xi^2 + \zeta^2 + 2l_{n2}\{\xi \cos\Theta_3 + \zeta \sin\Theta_3\} - 2\, l_{j2}(\xi - l_{n2} \cos\Theta_3) + l_{n2}^2 + l_{j2}^2,$$
$$\dot{f}_{4c} = \xi\,\dot{\xi} + \zeta\,\dot{\zeta} + l_{n2}\{\dot{\xi} \cos\Theta_3 - \xi \sin\Theta_3 \cdot \Theta_3 + \dot{\zeta} \sin\Theta_3 + \zeta \cos\Theta_3 \cdot \dot{\Theta}_3\}$$
$$- l_{j2}(\dot{\xi} + l_{n2} \sin\Theta_3 \cdot \dot{\Theta}_3),$$
$$\delta_{4c0} = [(\xi_0 + l_{n2} \cos\Theta_{30} - l_{j2})^2 + (\zeta_0 + l_{n2} \sin\Theta_{30})]^{1/2},$$

$$\delta_5 = \sqrt{f_5(\xi, \zeta, \Theta_3, \Theta_4)} - \delta_{50}, \quad l_c = l_o + l_p \cos\beta, \quad l_d = l_q - l_p \sin\beta,$$
$$f_5 = \xi^2 + \zeta^2 + 2(l_4 + l_5)\{(\xi - l_c) \cos\Theta_3 + (\zeta + l_d) \sin\Theta_3\}$$
$$+ 2(l_6 + l_7)\{(\xi - l_c) \cos\Theta_4 + (\zeta + l_d) \sin\Theta_4\} + 2(l_4 + l_5)(l_6 + l_7) \cos(\Theta_3 - \Theta_4)$$
$$+ 2l_d\zeta - 2l_c\xi + l_c^2 + l_d^2 + (l_4 + l_5)^2 + (l_6 + l_7)^2,$$

$$\dot{f}_5 = \xi\ddot{\xi} + \zeta\ddot{\zeta} + (l_4 + l_5)\{\ddot{\xi}\cos\Theta_3 - (\xi - l_c)\sin\Theta_3 \cdot \dot{\Theta}_3 + \dot{\zeta}\sin\Theta_3 + (\zeta + l_d)\cos\Theta_3 \cdot \dot{\Theta}_3\}$$
$$+ (l_6 + l_7)\{\ddot{\xi}\cos\Theta_4 - (\xi - l_c)\sin\Theta_4 \cdot \dot{\Theta}_4 + \dot{\zeta}\sin\Theta_4 + (\zeta + l_d)\cos\Theta_4 \cdot \dot{\Theta}_4\}$$
$$+ l_d\ddot{\zeta} - l_c\ddot{\xi} + (l_4 + l_5)(l_6 + l_7)\{\sin(\Theta_3 - \Theta_4) \cdot (\dot{\Theta}_4 - \dot{\Theta}_3)\},$$
$$\delta_{50} = [\{\xi_0 + (l_4 + l_5)\cos\Theta_{30} + (l_6 + l_7)\cos\Theta_{40} - l_c\}^2$$
$$+ \{\zeta_0 + (l_4 + l_5)\sin\Theta_{30} + (l_6 + l_7)\sin\Theta_{40} + l_d\}^2]^{1/2}.$$

Here δ_{io}, $i = 1, 2, 3, 4, 5$ represent the nominal values of these variables.

Appendix C. Formulae for calculating the parameters in the stiffness and damping matrices of the linear model

C.1. Stiffness matrix elements of Eq. (8)

This matrix is symmetric and thus only the elements in the upper triangular part are given below.

$$K_{411} = \frac{k_1}{\delta_{10}^2}K_{11}^2 + \frac{k_2}{\delta_{20}^2}(\xi_0 - l_m\cos\Theta_{s0})^2 + \frac{k_4}{\delta_{k40}^2}K_{41}^2 + \frac{k_5}{\delta_{50}^2}(\xi_0 + K_{51})^2,$$

$$K_{412} = \frac{k_1}{\delta_{10}^2}K_{11}K_{12} + \frac{k_2}{\delta_{20}^2}(\xi_0 - l_m\cos\Theta_{s0})(\zeta_0 - l_m\sin\Theta_{s0})$$
$$+ \frac{k_4}{\delta_{k40}^2}K_{41}K_{42} + \frac{k_5}{\delta_{50}^2}(\xi_0 + K_{51})(\zeta_0 + K_{52}),$$

$$K_{413} = 0, \quad K_{414} = \frac{k_1}{\delta_{10}^2}K_{11}K_{13}(l_k - l_m), \quad K_{415} = \frac{k_4}{\delta_{k40}^2}K_{41}K_{43} + \frac{k_5K_{54}}{\delta_{50}^2}(\xi_0 + K_{51}),$$

$$K_{416} = \frac{k_5K_{55}}{\delta_{50}^2}(\xi_0 + K_{51}),$$

$$K_{417} = \frac{k_1K_{11}K_{14}}{\delta_{10}^2} + \frac{k_2l_m(\xi_0 - l_m\cos\Theta_{s0})\{\xi_0\sin\Theta_{s0} - \varsigma_0\cos\Theta_{s0}\}}{\delta_{20}^2},$$

$$K_{422} = \frac{k_1}{\delta_{10}^2}K_{12}^2 + \frac{k_2}{\delta_{20}^2}(\zeta_0 - l_m\sin\Theta_{s0})^2 + k_3 + \frac{k_4}{\delta_{k40}^2}K_{42}^2 + \frac{k_5}{\delta_{50}^2}(\zeta_0 + K_{52})^2,$$

$$K_{423} = 0, \quad K_{424} = \frac{k_1}{\delta_{10}^2}K_{12}K_{13}(l_k - l_m),$$
$$K_{425} = \frac{k_3l_{nj31}K_{\Theta_3}}{\delta_{30}} + \frac{k_4}{\delta_{k40}^2}K_{42}K_{43} + \frac{k_5K_{54}}{\delta_{50}^2}(\zeta_0 + K_{52}),$$

$$K_{426} = \frac{k_5 K_{55}}{\delta_{50}^2}(\zeta_0 + K_{52}), \quad K_{427} = \frac{k_1 K_{12} K_{14}}{\delta_{10}^2} + \frac{k_2 l_m(\varsigma_0 - l_m \sin \Theta_{s0})\{\xi_0 \sin \Theta_{s0} - \varsigma_0 \cos \Theta_{s0}\}}{\delta_{20}^2},$$

$$K_{43i} = 0 \quad (i = 1, \ldots, 7),$$

$$K_{444} = \frac{k_1}{\delta_{10}^2} K_{13}^2 (l_k - l_m)^2, \quad K_{445} = 0, \quad K_{446} = 0, \quad K_{447} = \frac{k_1 (l_k - l_m) K_{13} K_{14}}{\delta_{10}^2},$$

$$K_{455} = \frac{k_3 K_{\Theta_3}^2}{\delta_{30}^2} + \frac{k_4}{\delta_{k40}^2} K_{43}^2 + \frac{k_5}{\delta_{50}^2} K_{54}^2, \quad K_{456} = \frac{k_5}{\delta_{50}^2} K_{54} K_{55},$$

$$K_{457} = 0, \quad K_{466} = \frac{k_5}{\delta_{50}^2} K_{55}^2, \quad K_{467} = 0,$$

$$K_{477} = \frac{k_1 K_{14}^2}{\delta_{10}^2} + k_s + \frac{k_2 l_m^2 \{\xi_0 \sin \Theta_{s0} - \varsigma_0 \cos \Theta_{s0}\}^2}{\delta_{20}^2}.$$

C.2. Damping matrix elements of Eq. (8)

This matrix is also symmetric and thus only the elements in the upper triangular part are given below. The subscript notation, when including a 0 indicates the initial configuration value of the variable, about which the expansions were performed.

$$C_{411} = \frac{c_1}{\delta_{10}^2} K_{11}^2 + \frac{c_2}{\delta_{20}^2}(\xi_0 - l_m \cos \Theta_{s0})^2 + \frac{c_4}{\delta_{c40}^2} C_{41}^2 + \frac{c_5}{\delta_{50}^2}(\xi_0 + K_{51})^2,$$

$$C_{412} = \frac{c_1}{\delta_{10}^2} K_{11} K_{12} + \frac{c_2}{\delta_{20}^2}(\xi_0 - l_m \cos \Theta_{s0})(\zeta_0 - l_m \sin \Theta_{s0}) + \frac{c_4}{\delta_{c40}^2} C_{41} C_{42} + \frac{c_5}{\delta_{50}^2}(\xi_0 + K_{51})(\zeta_0 + K_{52}),$$

$$C_{413} = 0, \quad C_{414} = \frac{c_1}{\delta_{10}^2} K_{11} K_{13}(l_k - l_m), \quad C_{415} = \frac{c_4}{\delta_{c40}^2} C_{41} C_{43} + \frac{c_5 K_{54}}{\delta_{50}^2}(\xi_0 + K_{51}),$$

$$C_{416} = \frac{c_5 K_{55}}{\delta_{50}^2}(\xi_0 + K_{51}), \quad C_{417} = \frac{c_1 K_{11} K_{14}}{\delta_{10}^2} + \frac{c_2 l_m(\xi_0 - l_m \cos \Theta_{s0})\{\xi_0 \sin \Theta_{s0} - \varsigma_0 \cos \Theta_{s0}\}}{\delta_{20}^2},$$

$$C_{422} = \frac{c_1}{\delta_{10}^2} K_{12}^2 + \frac{c_2}{\delta_{20}^2}(\zeta_0 - l_m \sin \Theta_{s0})^2 + c_3 + \frac{c_4}{\delta_{c40}^2} C_{42}^2 + \frac{c_5}{\delta_{50}^2}(\zeta_0 + K_{52})^2, \quad C_{423} = 0,$$

$$C_{424} = \frac{c_1}{\delta_{10}^2} K_{12} K_{13}(l_k - l_m), \quad C_{425} = \frac{c_3 l_{nj31} K_{\Theta_3}}{\delta_{30}} + \frac{c_4}{\delta_{c40}^2} C_{42} C_{43} + \frac{c_5 K_{54}}{\delta_{50}^2}(\zeta_0 + K_{52}),$$

$$C_{426} = \frac{c_5 K_{55}}{\delta_{50}^2}(\zeta_0 + K_{52}), \quad C_{427} = \frac{c_1 K_{12} K_{14}}{\delta_{10}^2} + \frac{c_2 l_m(\varsigma_0 - l_m \sin \Theta_{s0})\{\xi_0 \sin \Theta_{s0} - \varsigma_0 \cos \Theta_{s0}\}}{\delta_{20}^2},$$

$$C_{433} = T_{1_{max}} = 22.4642, \quad C_{434} = -T_{1_{max}} = -22.4642, \quad C_{43i} = 0 \quad (i = 5, 6, 7)$$

$$C_{444} = \frac{c_1}{\delta_{10}^2} K_{13}^2 (l_k - l_m)^2 + T_{1_{max}} + T_{2_{max}}, \quad C_{445} = -T_{2_{max}},$$

$$C_{446} = 0, \quad C_{447} = \frac{c_1 (l_k - l_m) K_{13} K_{14}}{\delta_{10}^2},$$

$$C_{455} = \frac{c_3 K_{\Theta_3}^2}{\delta_{30}^2} + \frac{c_4}{\delta_{c40}^2} C_{43}^2 + \frac{k_5}{\delta_{50}^2} K_{54}^2 + T_{2_{max}} + T_{3_{max}}, \quad C_{456} = \frac{c_5}{\delta_{50}^2} K_{54} K_{55} - T_{3_{max}}, \quad C_{457} = 0,$$

$$C_{466} = \frac{c_5}{\delta_{50}^2} K_{55}^2 + T_{3_{max}}, \quad C_{467} = 0,$$

$$C_{477} = \frac{c_1 K_{14}^2}{\delta_{10}^2} + \frac{c_2 l_m^2 \{\xi_0 \sin \Theta_{s0} - \varsigma_0 \cos \Theta_{s0}\}^2}{\delta_{20}^2}.$$

C.3. Parameters used in stiffness and damping elements

The parameters not defined in Appendices C.1 and C.2 are listed below.

$$K_{\Theta_3} = \Delta \left(\varsigma_0 + \frac{\Delta}{\cos \Theta_{30}} \sin \Theta_{30} \right),$$

$$K_{11} = \xi_0 + (l_k - l_m) \cos \Theta_{20} - l_k \cos \Theta_{s0}, \quad K_{12} = \zeta_0 + (l_k - l_m) \sin \Theta_{20} - l_k \sin \Theta_{s0},$$

$$K_{13} = \zeta_0 \cos \Theta_{20} - \xi_0 \sin \Theta_{20} - l_k \sin(\Theta_{s0} - \Theta_{20}),$$
$$K_{41} = l_{n1} \cos \Theta_{30} + \xi_0 - l_{j1}, \quad K_{42} = l_{n1} \sin \Theta_{30} + \zeta_0,$$

$$K_{43} = l_{n1} \{ l_{j1} \sin \Theta_{30} + \zeta_0 \cos \Theta_{30} - \xi_0 \sin \Theta_{30} \},$$

$$C_{41} = l_{n2} \cos \Theta_{30} + \xi_0 - l_{j2}, \quad C_{42} = l_{n2} \sin \Theta_{30} + \zeta_0,$$
$$C_{43} = l_{n2} \{ l_{j2} \sin \Theta_{30} + \zeta_0 \cos \Theta_{30} - \xi_0 \sin \Theta_{30} \},$$

$$K_{51} = (l_4 + l_5) \cos \Theta_{30} + (l_6 + l_7) \cos \Theta_{40} - l_c,$$
$$K_{52} = (l_4 + l_5) \sin \Theta_{30} + (l_6 + l_7) \sin \Theta_{40} + l_d,$$

$$K_{54} = (l_4 + l_5) \{ (\zeta_0 + K_{52}) \cos \Theta_{30} - (\xi_0 + K_{51}) \sin \Theta_{30} \},$$

$$K_{55} = (l_6 + l_7) \{ (\zeta_0 + K_{52}) \cos \Theta_{40} - (\xi_0 + K_{51}) \sin \Theta_{40} \}.$$

References

[1] M.J. Griffin, Handbook of Human Vibration, Academic Press, New York, 1990.
[2] M.H. Pope, H. Broman, T. Hannsson, The dynamic response of a subject seated on various cushions, Ergonomics 32 (10) (1989) 1155–1166.

[3] M.J. Griffin, The evaluation of vehicle vibration and seats, Applied Ergonomics 9 (1) (1978) 15–21.
[4] M.J. Griffin, E.M. Whitham, K.C. Parsons, Vibration and comfort I. Translational seat vibration, Ergonomics 25 (7) (1982) 603–630.
[5] C. Corbridge, M.J. Griffin, Vibration and comfort: vertical and lateral motion in the range 0.5–5.0 Hz, Ergonomics 29 (2) (1986) 249–272.
[6] K.D. Cavender, Real time foam performance testing, Journal of Cellular Plastics 29 (1993) 350–364.
[7] J.W. Leenslag, E. Huygens, A. Tan, Recent advances in the development and characterisation of automotive comfort seating foams, Cellular Polymers 16 (4) (1997) 411–430.
[8] N.C. Hilyard, W.L. Lee, A. Cunningham, Energy dissipation in polyurethane cushion foams and its role in dynamics ride comfort, Conference on Cellular Polymers, Forum Hotel, London, UK, 1991, pp. 187–191.
[9] A. Cunningham, E. Huygens, J.W. Leenslag, MDI comfort cushioning for automotive applications, Cellular Polymers 13 (6) (1994) 461–472.
[10] W.N. Patten, S. Sha, C. Mo, A vibration model of open celled polyurethane foam automotive seat cushions, Journal of Sound and Vibration 217 (1) (1998) 145–161.
[11] S.W. White, S.K. Kim, A.K. Bajaj, P. Davies, D.K. Showers, P.E. Liedtke, Experimental techniques and identification of nonlinear and viscoelastic properties of flexible polyurethane foam, Nonlinear Dynamics 22 (2000) 281–313.
[12] J.C. Moreland, G.L. Wilkes, R.B. Turner, Viscoelastic behaviour of flexible slabstock polyurethane foam as a function of temperature and relative humidity. I. Tensile and compression stress (load) relaxation, Journal of Applied Polymer Science 52 (1994) 549–568.
[13] J.C. Moreland, G.L. Wilkes, R.B. Turner, Viscoelastic behaviour of flexible slabstock polyurethane foam as a function of temperature and relative humidity. II. Compressive creep behaviour, Journal of Applied Polymer Science 52 (1994) 569–576.
[14] S.D. Smith, Limitations in predicting human vibration response characteristics from manikins and rigid body masses, Progress with Human factors in Automotive Design: Seating Comfort, Visibility, and Safety, Vol. 1242, SAE Special Publication, SAE, Warrendale, PA, USA, 1997, pp. 169–199.
[15] Y. Gu, Comparison test of transmissibility response from human occupant and anthropodynamic mannequin, Progress with Human factors in Automotive Design: Driving, Vehicle Seating, and Rear Vision, Vol. 1358, SAE Special Publication, SAE, Warrendale, PA, USA, 1998, pp. 71–73.
[16] J.H. Varterasian, R.R. Thompson, The dynamic characteristics of automobile seats with human occupants, 1978 SAE Technical Paper Series Paper No. 770249, SAE, Warrendale, PA.
[17] S.W. White, Dynamic Modelling and Measurement of Occupied Seats and Seating Foam, Master Thesis, Purdue University, 1998.
[18] S.W. White, S.K. Kim, P. Davies, A.K. Bajaj, P.E. Liedtke, D.K. Showers, Modelling and measurement of occupied car seats, Paper No. 1999-01-1690, SAE Noise and Vibration Conference, Traverse City, MI, May 17–20, 1999.
[19] S. Nishiyama, F. Takeda, T. Takeshima, Influences of sitting posture on vibration characteristics of the human body (experimental investigation), Japan Society of Mechanical Engineers 61 (590) (1995) 3866–3873.
[20] S. Nishiyama, Development of simulation system on vehicle-occupant dynamic interaction (1st Report, Theoretical analysis and system verification), Transactions of the Japan Society of Mechanical Engineers C 59 (568) (1993) 3613–3621.
[21] S. Nishiyama, Development of simulation system on vehicle-occupant dynamic interaction (2nd Report, Influence of sitting posture on human comfort), Transactions of the Japan Society of Mechanical Engineers C 59 (568) (1993) 3622–3629.
[22] S. Nishiyama, Development of simulation system on vehicle-occupant dynamic interaction (3rd Report, Influence of parameters of occupant-seat system on human comfort), Transactions of the Japan Society of Mechanical Engineers C 60 (573) (1994) 1509–1516.
[23] S. Nishiyama, Vertical and lateral vibration analysis of vehicle-occupant dynamic interaction with simulation system, Transactions of the Japan Society of Mechanical Engineers C 59 (567) (1993) 3239–3246.
[24] R. Muksian, C.D. Nash, A model for the response of seated humans to sinusoidal displacements of the seat, Journal of Biomechanics 7 (1974) 209–215.

[25] F.M. Amirouche, Modelling of human reactions to whole-body vibration, Journal of Biomechanical Engineering 109 (1987) 210–217.
[26] F.M. Amirouche, M. Xie, A. Patwardhan, Optimization of the contact damping and stiffness coefficients to minimize human body vibration, Journal of Biomechanical Engineering 116 (1994) 413–420.
[27] M. Demic, Optimization of vehicles elasto-damping elements characteristics from the aspect of ride comfort, Vehicle System Design 23 (1994) 351–377.
[28] E. Berger, B.J. Gilmore, Seat dynamic parameters for ride quality, SAE Transactions, Journal of Passenger Cars 102 (8) (1993) 204–217.
[29] Y. Wan, J.M. Schimmels, Optimal seat suspension design based on minimum simulated subjective response, Journal of Biomedical Engineering 119 (1997) 409–416.
[30] P.É. Boileau, S. Rakheja, X. Yang, I. Stiharu, Comparison of biodynamic response characteristics of various human body models as applied to seated vehicle drivers, Noise and Vibration Worldwide October 1997 (1997) 7–14.
[31] W.N. Patten, J. Pang, Validation of a nonlinear automotive seat cushion vibration model, Vehicle System Dynamics 30 (1998) 55–68.
[32] N.J. Mansfied, M.J. Griffin, Non-linearities in apparent mass and transmissibility during exposure to whole-body vertical vibration, Journal of Biomechanics 33 (2000) 933–941.
[33] V.P. Tregoubov, Problems of mechanical model identification for human body under vibration, Mechanisms and Machine Theory 35 (2000) 491–504.
[34] J.S. Bendat, A.G. Piersol, Random Data, Analysis and Measurement Procedures, Wiley, New York, 1986.
[35] P. Davies, J.K. Hammond, A comparison of Fourier and parametric methods for structural system identification Transactions of the American Society of Mechanical Engineers, Journal of Vibration, Acoustics, Stress and Reliability in Design 106 (1984) 40–48.
[36] S.H. Beckaitis, H.J. Mertz (Ed.), Hybrid III: The first human-like crash test dummy, PT-44, Society of Automotive Engineering Inc., Warrendale, PA, 1993.